

# Kinetics of Turn-offs of Frog Rod Phototransduction Cascade

Luba A. Astakhova, Michael L. Firsov, and Victor I. Govardovskii

Sechenov Institute for Evolutionary Physiology & Biochemistry, Russian Academy of Sciences, 194223 St. Petersburg, Russia

The time course of the light-induced activity of phototransduction effector enzyme cGMP-phosphodiesterase (PDE) is shaped by kinetics of rhodopsin and transducin shut-offs. The two processes are among the key factors that set the speed and sensitivity of the photoresponse and whose regulation contributes to light adaptation. The aim of this study was to determine time courses of flash-induced PDE activity in frog rods that were dark adapted or subjected to nonsaturating steady background illumination. PDE activity was computed from the responses recorded from solitary rods with the suction pipette technique in  $\text{Ca}^{2+}$ -clamping solution.

A flash applied in the dark-adapted state elicits a wave of PDE activity whose rising and decaying phases have characteristic times near 0.5 and 2 seconds, respectively. Nonsaturating steady background shortens both phases roughly to the same extent. The acceleration may exceed fivefold at the backgrounds that suppress  $\approx 70\%$  of the dark current.

The time constant of the process that controls the recovery from super-saturating flashes (so-called dominant time constant) is adaptation independent and, hence, cannot be attributed to either of the processes that shape the main part of the PDE wave. We hypothesize that the dominant time constant in frog rods characterizes arrestin binding to rhodopsin partially inactivated by phosphorylation. A mathematical model of the cascade that considers two-stage rhodopsin quenching and transducin inactivation can mimic experimental PDE activity quite well. The effect of light adaptation on the PDE kinetics can be reproduced in the model by concomitant acceleration on both rhodopsin phosphorylation and transducin turn-off, but not by accelerated arrestin binding. This suggests that not only rhodopsin but also transducin shut-off is under adaptation control.

## INTRODUCTION

Absorption of light by rhodopsin molecules in the photoreceptor outer segment translates into hyperpolarization of the entire cell by biochemical amplification cascade that uses cGMP as the second messenger. Free cGMP level in the rod outer segment (ROS) cytoplasm is set by interplay between two enzymes, cGMP-producing guanylate cyclase and cGMP-degrading phosphodiesterase. Light activates cGMP phosphodiesterase (PDE), thereby decreasing the cGMP level and leading to the closure of the cationic channels of the ROS plasma membrane. Activation of PDE by light is a multistep process. First, the rhodopsin molecule switches to its active state after catching a photon. In this state, rhodopsin activates many molecules of the specific photoreceptor G protein transducin. Transducin, in turn, binds to PDE and stimulates its hydrolytic activity.

Restoration of the pre-stimulus level of cGMP is mandatory for recovery of rod current to make the cell capable of reacting to new light stimuli. This means that the PDE activity must return to its “dark” level, that is, the cascade must be quenched. Serial activation of transducins by rhodopsin is progressively slowed down by rhodopsin phosphorylation, and then completely

stopped by arrestin binding. PDE activates when it combines with transducin  $\alpha$  subunit ( $T_\alpha^*$ ) bearing GTP. The inactivation occurs when  $T_\alpha\text{GTP}^*\text{PDE}$  complex hydrolyzes GTP to GDP. Inactivation of the cascade and restoration of the dark state is under the control of negative  $\text{Ca}^{2+}$  feedback that operates mostly by increasing the speed of rhodopsin phosphorylation and stimulating cGMP production (for review see Pugh and Lamb 2000; Burns and Baylor 2001; Burns and Arshavsky 2005; Chen, 2005; Bush and Makino 2007).

Thus, the time courses of PDE activation and inactivation are the key factors that control both the speed of the photoreaction and the restoration of the dark-adapted state. Surprisingly, there is not much data on these processes obtained in direct physiological experiments. Rates of the reactions measured *in vitro* are usually low and poorly compatible with the observed speed of physiological response. For instance, intrinsic GTPase activity of transducin is too low to ensure timely turn-off of the cascade (Chabre and Deterre, 1989; Arshavsky and Bownds, 1992; Angleson and Wensel, 1993). Discovery of RGS9-1, a GTPase-activating protein (GAP) that greatly accelerates transducin GTPase, improved the situation (Nekrasova et al., 1997; He et al., 1998;

Correspondence to Michael L. Firsov: firsov@iephb.nw.ru

Abbreviations used in this paper: GAP, GTPase-activating protein; IBMX, 3-isobutyl-1-methylxanthine; PDE, cGMP phosphodiesterase; ROS, rod outer segment.

© 2008 Astakhova et al. This article is distributed under the terms of an Attribution-Noncommercial-Share Alike-No Mirror Sites license for the first six months after the publication date (see <http://www.jgp.org/misc/terms.shtml>). After six months it is available under a Creative Commons License (Attribution-Noncommercial-Share Alike 3.0 Unported license, as described at <http://creativecommons.org/licenses/by-nc-sa/3.0/>).

Chen et al., 2000). By genetically manipulating the level of expression of the GAP complex, Krispel et al. (2006) have demonstrated that in normal mouse rods transducin turn-off occurs with the time constant  $\tau_E \approx 0.2$  s. In amphibian rods,  $\tau_E$  was estimated to be 2–3 s (Pepperberg et al., 1992, 1994; Lyubarsky et al., 1996; Sagoo and Lagnado, 1997; Nikonov et al., 1998; Calvert et al., 2002). However, the GAP effect of RGS9 strongly depends on its concentration/level of expression both in vitro (Makino et al., 1999; Arshavsky et al., 2002) and in vivo (Krispel et al., 2006), so the actual rate of transducin shut-off in species other than mice or salamander remains uncertain.

Similarly, physiological quenching of rhodopsin activity occurs in less than a second, whereas phosphorylation in tube usually proceeds on a minute time scale (Wilden et al., 1986; Gorodovikova et al., 1994; Calvert et al., 1998; Kennedy et al., 2003, among many others).

The rates of the two turn-off processes were also inferred from various mathematical models of phototransduction (Lyubarsky et al., 1996; Nikonov et al., 2000; Hamer, 2000a, 2000b; Hamer et al., 2003, 2005; Kuzmin et al., 2004; Caruso et al., 2006). These models inevitable include several parameters whose values are poorly known, so the reliability of the values of time constants of rhodopsin and PDE quenching ( $\tau_R$  and  $\tau_E$ ) extracted from modeling is quite uncertain. Thus, obtaining a direct physiological estimate of  $\tau_R$  and  $\tau_E$  may impose constraints on the structure of the models and on values of other parameters that are derived from modeling.

Activation and subsequent quenching of rhodopsin and transducin result in a wave of PDE activity whose time course is determined by the kinetics of rhodopsin and transducin shut-offs. The aim of this study was to restore the waveform of flash-induced PDE activity from the photoresponses of an intact rod. Then we planned to extract  $\tau_R$  and  $\tau_E$  values from the curve and investigate possible effects of light adaptation on them. The PDE time course was determined from photoresponses of isolated frog rods to dim (nonsaturating) flashes recorded under  $\text{Ca}^{2+}$ -clamped conditions. This procedure fixes the cytoplasmic free calcium concentration at the pre-stimulus level thereby canceling powerful dynamic calcium feedbacks to many components of the phototransduction cascade (Matthews et al., 1988; Nakatani and Yau, 1988). Excluding feedbacks greatly simplifies the equations that relate the cell current response to the PDE activity, thus enabling restoration of underlying light-induced PDE waveform.

We found that it is not possible to unambiguously extract characteristic times of two turn-off processes and attribute them specifically to rhodopsin and transducin quenching. However, we show that steady background illumination that leads to the closure of 15–70% of channels and to corresponding decrease in intracellular cal-

cium accelerates the processes that shape both the rising and falling phases of the PDE response by more than fivefold. This suggests that, contrary to the current belief, not only rhodopsin but also transducin shut-off is under adaptation control.

On the other hand, the so-called dominant time constant determined from Pepperberg analysis (Pepperberg et al., 1992) ( $\tau_D \approx 2$  s) was adaptation independent. This means that the main phase of either rhodopsin or transducin turn-off is not the process that underlies  $\tau_D$  and controls the recovery from saturation in the frog rod.

## MATERIALS AND METHODS

### Experimental Procedure

Experiments were performed on retinas of *Rana ridibunda* frogs caught in the wild. Frogs were treated in accordance with the Council for International Organizations of Medical Sciences principles for biomedical research involving animals (1985). Animals were kept for up to 6 months in tanks with free access to water at 20–25°C on a natural day/night cycle, and fed living cockroaches and dry pet food. Before the experiment, animals were dark adapted overnight. Under dim red light the frogs were killed by decapitation and pithed. Retinas were removed under infrared surveillance, and isolated rods were obtained as described by Firsov et al. (2005). Photoreceptor current was recorded using a standard suction pipette recording technique (Baylor et al., 1979). Rod was sucked into a glass pipette in the configuration, *inner segment in*.

To quickly change the ionic milieu around the rod outer segment, we used an assembly of movable tubings. A two-barrel pipette made of a theta capillary produced two jets of solutions of different composition. The second, single-barrel pipette placed opposite to the theta tubing at the distance of  $\sim 0.5$  mm sucked the jets in, thus preventing their mixing with the main bath solution that was always perfused with slowly flowing normal Ringer. The rod in the recording pipette was originally placed into the main bath close to the two jets. A computer-controlled stepper motor could then move the tubing assembly so that the rod was suddenly immersed into either of the two jets of different composition. The direction of the jets was at  $\sim 45^\circ\text{C}$  to the rod axis to reduce mechanical effects on the cell.

Light-stimulation system consisted of two independent channels based on high-output LEDs with  $\lambda_{\text{max}} = 525$  nm. Stimulus intensity was controlled by switchable ND filters and LED current. Typically, we used 10-ms flashes to stimulate the rod. Flash intensity expressed as the number of isomerizations per flash ( $R^*$ ) was calibrated for each individual rod using the statistics of few-photon responses (Baylor et al., 1979). Cell dimensions were determined from the IR monitor screen, the number of rhodopsin molecules per ROS calculated assuming rhodopsin concentration of 3.2 mM, and intensity expressed as the fractional bleach, if necessary. Independently, intensity of impinging light  $I$  was calibrated in photons  $\cdot \mu\text{m}^{-2}\text{s}^{-1}$  using Burr-Brown OPT-310 integrated optosensor. It could be converted into  $R^*$  using the rod light-collecting area  $S$  (Baylor et al., 1979, Eq. 14):

$$S = \frac{\pi d^2 l}{4} \cdot q \cdot \ln(10) \cdot f \cdot \alpha_{525}.$$

Here,  $d$  is the ROS diameter,  $l$  is the ROS length,  $q = 0.67$  is the quantum yield of rhodopsin bleaching, and  $\alpha_{525} = 0.015 \mu\text{m}^{-1}$  is the specific axial pigment density at 525 nm (as estimated from

our MSP recordings). Factor  $f = 0.5$  applies to the situation when ROS is illuminated side-on with nonpolarized light. The two calibrations coincided within 20%. Accumulated bleach by stimulating flashes and background light did not exceed 0.5% throughout the experiment, so no correction for rhodopsin loss was made.

Photoresponses were low-pass filtered at 30 Hz (8-pole Bessel filter), digitized at 100 Hz, and stored on the computer hard disk. If necessary, further digital filtering could be applied to the data. Data acquisition, stimulus timing, and stimulus intensity were under LabView software control (National Instruments).

Standard Ringer solution used for retinal dissection and as the main solution in the perfusion bath contained (in mM): 90 NaCl, 2.5 KCl, 1.6 MgSO<sub>4</sub>, 10 glucose, 1 CaCl<sub>2</sub>, 5 NaHCO<sub>3</sub>, 5 HEPES, and 50 mg/l bovine serum albumin, pH adjusted to 7.6. As for the solution to block Ca<sup>2+</sup> feedback onto the cascade, we tested various replacements for Na<sup>+</sup> used in previous works: guanidinium<sup>+</sup> (Nakatani and Yau, 1988; Matthews et al., 1988, 1990; Fain et al., 1989), Li<sup>+</sup> (Matthews et al., 1990), and choline<sup>+</sup> (Matthews, 1995; Lyubarsky et al., 1996; Nikonov et al., 1998; Matthews and Fain, 2001). Although guanidinium<sup>+</sup> and Li<sup>+</sup> yielded usable results, multiple exposures to these solutions were irreversibly damaging to rods. Most reproducible photoresponses and best stability of [Ca<sup>2+</sup>]<sub>in</sub> were obtained in the Ca<sup>2+</sup>-clamping solution after Lyubarsky et al. (1996) and Nikonov et al. (1998). It contained (in mM): 90 choline chloride, 5 choline bicarbonate, 10 glucose, 50 mg/l bovine serum albumin, and 5 HEPES, pH brought to 7.6 by TMA-OH. Free calcium level was set to nominally 3.4 nM by 0.4 mM CaCl<sub>2</sub> plus 2 mM EGTA.

All computations were performed with MathCad 2001i (MathSoft).

### Theoretical Basis of Determining Light-induced PDE Activity from Ca-clamped Responses

Equations used here were previously introduced in various forms by many researchers. For uniformity, we will further follow, when possible, the formulations and notation by Pugh and Lamb (2000).

Current  $j$  flowing through the cGMP-gated channels of the ROS plasma membrane at any moment of time and registered by the suction pipette is given by:

$$j(t) = F \frac{[cg]^{n_{cG}}}{[cg]^{n_{cG}} + K^{n_{cG}}}, \quad (1)$$

where  $F$  is a proportionality coefficient,  $[cg]$  is the concentration of cyclic GMP,  $K$  is the half-saturation constant, and  $n_{cG} = 2-3$  is the Hill's coefficient that relates the conductivity of the membrane to the cGMP concentration (Fesenko et al., 1985; Haynes et al., 1986; Zimmerman and Baylor, 1986). Because in normal conditions  $[cg] \ll K$  Eq. 1 simplifies to:

$$j(t) = F_1 \cdot [cg(t)]^{n_{cG}}, \quad (1a)$$

the light response is:

$$r(t) = j_d - j(t), \quad (2)$$

where  $j_d$  is the dark current obtained from Eq. 1a by setting  $[cg(t)] = [cg_d]$  (here and throughout, the index  $d$  refers to the dark-adapted state).

Then the fractional response is given by:

$$r(t)/r_{\max} = 1 - (cG(t))^{1/n_{cG}},$$

where  $cG(t)$  is the cGMP concentration normalized to its dark level. After rearrangement of terms,

$$cG(t) = (1 - r(t)/r_{\max})^{1/n_{cG}}. \quad (3)$$

In the absence of feedbacks  $n_{cG}$  is constant, so the flash response recorded in Ca<sup>2+</sup>-clamping solution provides the time course of the cGMP concentration  $cG(t)$  and its time derivative,  $dcG(t)/dt$ .

On the other hand, the cGMP turnover is described by:

$$\frac{dcG(t)}{dt} = \alpha(t) - \beta(t) \cdot cG(t), \quad (4)$$

where  $\alpha(t)$  is the guanylate cyclase activity and  $\beta(t)$  is the rate of turnover of the cytoplasmic cGMP pool by PDE expressed in s<sup>-1</sup>.  $\beta(t) = \beta_d + \beta_f(t)$ , a sum of the PDE activity in darkness and an additional activity induced by light. In turn,  $\beta_f(t) = \beta_s(t) + \beta_{fl}(t)$ , where  $\beta_s(t)$  is the activity elicited by a steady background (if present), and  $\beta_{fl}(t)$  is the flash-induced activity. Due to normalization,  $cG(0) = 1$ , and  $\alpha(0) = \alpha_d = \beta_d$ .

Generally,  $\alpha(t)$  is under Ca feedback control and hence varies during photoresponse. However, in the absence of feedback  $\alpha(t)$  is constant at  $\alpha_d$ . Solving Eq. 4 for  $\beta_f(t)$ , one gets:

$$\beta_f(t) = \frac{1}{cG(t)} \left( \beta_d - \frac{dcG(t)}{dt} \right) - \beta_d. \quad (5)$$

Its equivalent has earlier been obtained (Rieke and Baylor, 1998, their Eq. 14).

It is evident from Eq. 3 and Eq. 5 that to calculate  $\beta_f(t)$  two parameters must be known, namely channels' cooperativity  $n_{cG}$  and dark cGMP turnover rate  $\beta_d$ . Analysis of intensity dependence of Ca<sup>2+</sup>-clamped responses allows estimating the  $n_{cG}$  value (see Results). However, special experiments should be done to determine  $\beta_d$ .

### Measurements of PDE Dark Activity $\beta_d$

Methods for determining dark cGMP turnover rate  $\beta_d$  were suggested by Hodgkin et al. (1985) and Hodgkin and Nunn (1988). Because in a steady-state the rate of cGMP production is equal to the rate of its hydrolysis,  $\alpha_d = \beta_d$  and  $cG_d = 1$  after normalization. Hence, as follows from Eq. 4, instantaneously stopping one of the two reactions would result in exponential decrease ( $\alpha_d = 0$ ) or linear increase ( $\beta_d = 0$ ) of the  $cG$  level whose initial rate is equal to the  $cG$  dark turnover rate.

In our work, we inhibited cGMP hydrolysis by suddenly applying to the cell a high concentration of the PDE inhibitor 3-isobutyl-1-methylxanthine (IBMX) (Hodgkin and Nunn, 1988; Cobbs, 1991).

As follows from Eq. 4, in this case:

$$cG(t) = 1 + \alpha_d t = 1 + \beta_d t \quad (6)$$

$$j(t)/j_d = cG(t)^{n_{cG}}.$$

Therefore, jumping into the IBMX-containing solution and then plotting

$$(j(t)/j_d)^{1/n_{cG}}$$

versus time would yield a straight line whose slope is  $\beta_d$ .

### Determining the Dominant Time Constant of the Cascade Shut-off

Pepperberg et al. (1992) introduced a simple scheme of photo-transduction that allowed extracting the time constant of the

slowest turn-off process by analyzing the recovery of rod circulating current after bright saturating light flashes. In this scheme, light produces, with a certain gain, an active substance whose single-exponential removal controls the recovery from saturation. Then the time in saturation

$$T_{sat} = -C + \tau_D \cdot \ln(gI) \quad (7)$$

where  $g$  is the gain,  $I$  is the stimulus strength, and  $\tau_D$  is the time constant of the substance's removal.  $C$  is a constant whose value depends on the level to which the activity in the cascade should decay to allow a fixed level of recovery of the circulating current. Thus, the  $T_{sat}$  vs.  $\ln(I)$  plot should be a straight line whose slope yields  $\tau_D$ .

The time in saturation,  $T_{sat}$ , is defined as the time between the moment of flash and the recovery of a certain fixed level of circulating current. Routinely it is taken as the recovery of a constant fraction (say, 10%) of the steady current flowing before the flash. This allows comparison among cells whose dark current levels can vary greatly. However, if two states of the same cell (e.g., dark and light adapted) are to be compared, a fixed absolute level of the current recovery should be used. It ensures that the hydrolytic activity of the cascade, in the course of quenching, decayed to the same level regardless of the adaptation state of the cell. Therefore, we chose as the criterion level the recovery of 10% of the dark current and then fixed the absolute value (which normally was near 1.5 pA) for each given cell.

## RESULTS

### Measurements of PDE Dark Activity

The PDE rate was measured by instant transfer of the cell from normal Ringer solution into the jet of Ringer containing 0.5 mM IBMX. The cell was first stimulated with a saturating flash to determine the zero level of the ROS current in normal Ringer. After recovery of the dark current, the cell was exposed to the IBMX-containing jet that resulted in a fast approximately twofold increase of the current (Fig. 1 A). Plotting

$$(j(t)/j_d)^{1/n_{cG}}$$

versus time yields the curve whose initial linear part has a slope of  $3.4 \text{ s}^{-1}$  (Fig. 1 B). (Here, we assume  $n_{cG} = 3$ , as follows from further analysis). Four trials made with this cell gave averaged value for  $\beta_d = 3.7 \pm 0.4 \text{ s}^{-1}$  (mean  $\pm$  SD). Mean value for six cells yields  $\beta_d = 3.4 \pm 0.8 \text{ s}^{-1}$ .

### Testing the Quality of the $\text{Ca}^{2+}$ Clamp

Using Eq. 5 for determining light-induced PDE activity  $\beta_i(t)$  relies on the assumption that the rate of the cGMP synthesis,  $\alpha(t)$ , is kept constant at its pre-stimulus level. In turn, this means that  $[\text{Ca}^{2+}]_{in}$  should stay constant during the photoresponse. This is supposed to be achieved by eliminating  $\text{Ca}^{2+}$  influx by removing calcium from the bathing solution and stopping active  $\text{Ca}^{2+}$  efflux by replacing external  $\text{Na}^+$  with an ion that does not drive the exchanger. However, perfect  $\text{Ca}^{2+}$  clamp can never be achieved because the rod in the clamping solution is in a non-steady state. Direct control of  $[\text{Ca}^{2+}]_{in}$  levels with a  $\text{Ca}^{2+}$ -sensitive dye could not help much because the fluorescence analysis demands strong illumination, which precludes further physiological experiments on the same cell. However, stability of  $[\text{Ca}^{2+}]_{in}$  can be assessed by measuring dark current values at different moments after the jump into the clamping solution. Here, we essentially follow the approach of Lyubarsky et al. (1996).

The thin line in Fig. 2 A shows changes of the suction pipette current in darkness after jumping the cell into the  $\text{Ca}^{2+}$ -clamping jet. Because in this solution  $\text{Na}^+$  is substituted by choline $^+$ , the dark current is mostly carried by the outward flux of intracellular  $\text{K}^+$  and changes its sign (see Matthews, 1995, 1996, 1997; Lyubarsky et al., 1996).

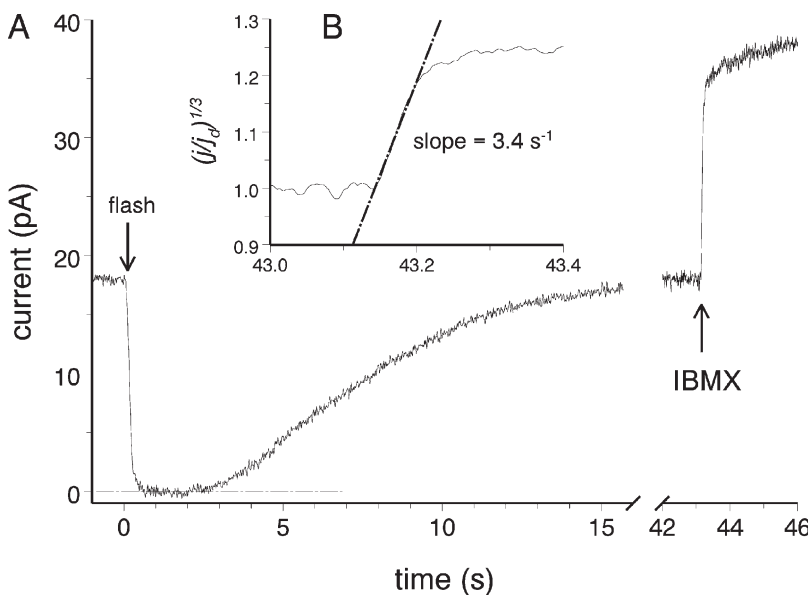


**Figure 1.** Determining dark cGMP turnover rate by IBMX application. (A) Saturating flash (downward arrow) is applied to determine zero level of the rod current. After recovery, the cell was instantaneously transferred to the jet of Ringer containing 0.5 mM IBMX (upward arrow). (B, inset) Current changes after IBMX application shown on an expanded time scale. Ordinate, cubic root of the current normalized to the dark level before the jump. Straight line is fit to the central part of the transition curve. Its slope is supposed to yield  $\beta_{dark}$ .



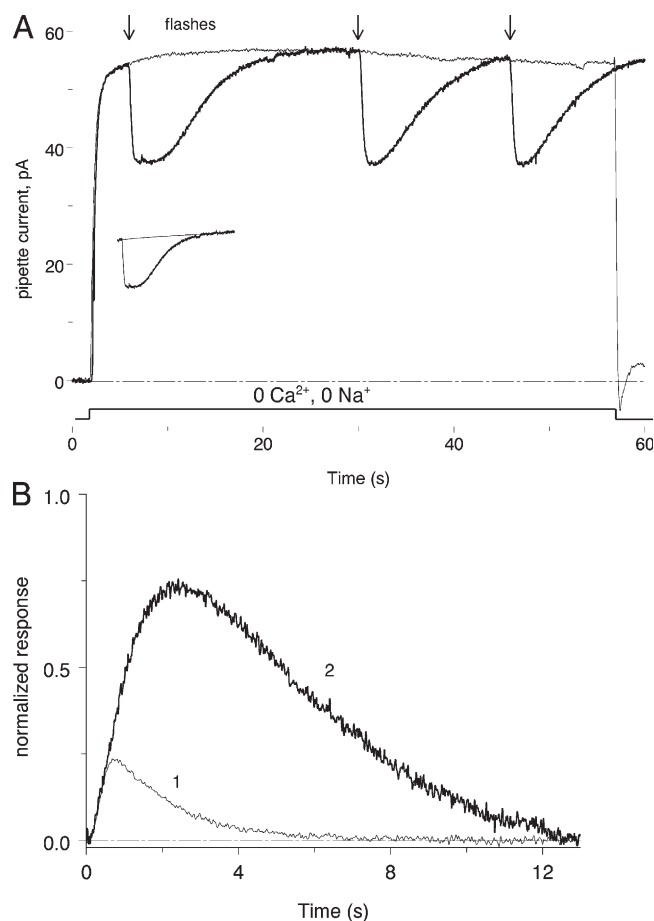


**Figure 2.** Testing the efficiency of the Ca<sup>2+</sup>-clamping procedure. (A) Assessing the stability of dark current in 0 Ca<sup>2+</sup>, 0 Na<sup>+</sup> solution. Zero level corresponds to the dark current in normal Ringer, and outward ROS current is plotted upward. Thin line shows changes in the pipette current after jumping the cell into 0 Ca<sup>2+</sup>, 0 Na<sup>+</sup> solution in darkness. After recovery of the dark current, the jump was repeated and the cell was stimulated with three saturating flashes (2,000 R\*, marked by arrows) to determine dark current (bold trace). The dark current rose by 15% between the first and second flashes, and then decreased back. 15% change of the dark current indicates the stability of [Ca<sup>2+</sup>]<sub>in</sub> within 1.9% (see Results). Inset shows the method for drawing zero level of the response. 2-s pre-flash stretch and 7-s stretch after the response termination are fitted with a cubic parabola (smooth thin line). (B) Assessing the feedback loop gain. Curve 1 is a response to a 13 R\* flash recorded in normal Ringer solution. Curve 2 is a response to the same flash in 0 Ca<sup>2+</sup>, 0 Na<sup>+</sup> solution. Ratio of time integrals of the two curves corrected for saturation provides an estimate of  $g_L$  (see Eq. 8). (A and B) Two different cells.

Shift of the junction potential and inversion of the dark current result in a fast current deviation that is followed with slow changes. The current completely recovers in <1 min after withdrawal to normal Ringer (not depicted). Then the jump is repeated, and saturating flashes are applied at various moments of time to determine the magnitude of the dark current. In this particular cell, the dark current first increased by ≈15% and then returned to its initial level. In other cells, we ob-

served slow changes of the dark current that could be of either direction.

Admittedly, Fig. 2 A shows one of the “best” recordings where two sequential jumps into 0 Ca<sup>2+</sup>, 0 Na<sup>+</sup> solution yielded virtually identical changes of the pipette dark current. More commonly, a series of jumps in darkness and during flash stimulation exhibited marked variability of dark pipette current among trials on the same cell. Therefore, to determine dark current level for each individual flash response, a 2-s stretch before the flash and an ≈10-s stretch after response termination were fitted by a cubic parabola, as shown in the inset in Fig. 2 A. The fitting curve was then used as zero level of photoreponse (dark current). All flash responses in Ca<sup>2+</sup>-clamping solution discussed further in this paper are processed this way.

The value of the dark current is a sensitive gauge of [Ca<sup>2+</sup>]<sub>in</sub>. Small fractional changes of [Ca<sup>2+</sup>]<sub>in</sub> translate into much bigger changes of the dark current due to cooperative control of guanylate cyclase by Ca<sup>2+</sup> and of the dark current channels by cGMP. Thus,

$$\frac{I_{d1}}{I_{d2}} = \left( \frac{[Ca^{2+}]_{in2}}{[Ca^{2+}]_{in1}} \right)^{n_{cG} \cdot n_{GC}},$$

where indices 1 and 2 refer to two states of the cell, and  $n_{GC}$  is Hill's coefficient of guanylate cyclase regulation by calcium (compare with Burns et al., 2002). The product  $n_{cG} \cdot n_{GC}$  is the steady-state gain of the feedback loop,  $g_L$ . Its value can be estimated from the ratio of time integrals (areas) of clamped/nonclamped responses,  $S_c/S_{nc}$  (Burns et al., 2002):

$$g_L = S_c / S_{nc} - 1 \approx n_{cG} \cdot n_{GC}. \quad (8)$$

For the raw responses of the cell shown in Fig. 2 B,  $S_c/S_{nc} = 9.3$  and  $g_L = 8.3$ . However, this value is an underestimate because Eq. 8 only holds for small responses within a linear range, which is not the case in Fig. 2 B. Nonlinearity can be taken into account by using Eqs. 1–5. Applying Eq. 5 to the curve 2 in Fig. 2 B, one can find the PDE waveform  $\beta_{fl}(t)$ . Then a “linearizing” factor  $f \gg 1$  can be introduced, and (imaginary) linear photoreponse to  $\beta_{fl}(t)/f$  computed using Eqs. 2–5. Further, a corrected  $S_c$  can be found as the time integral of the linear response multiplied by  $f$ . Similarly, normalized responses  $r(t)$  in normal Ringer, although close to the linear range, can approximately be corrected for saturation and corrected  $S_{nc}$  found by using the formula  $r_l(t) \approx r(t)/(1-r(t))$ , where  $r_l(t)$  is the “linearized” response. Here, Michaelis-like instantaneous saturation is assumed.

Such a correction yields  $g_L = 12.7$  for the responses shown in Fig. 2 B. The average of 53 pairs of clamped/nonclamped responses from 11 rods in a dark-adapted state gave  $g_L = 7.5 \pm 2.6$  (mean  $\pm$  SD, range 3.9–12.7). Background light that blocked 50–70% of dark current

reduced the loop gain to  $g_L = 5.2 \pm 1.6$  (mean  $\pm$  SD, range 2.0–8.3; 32 pairs of responses from eight cells).

Thus, our data suggest that the average  $n_{cG} n_{GC} = 7.5$  in frog rods. Therefore, the 15% increase of the dark current during 25 s elapsed between the first and second flash in Fig. 2 A is caused by just 1.9% decrease in  $[Ca^{2+}]_{in}$ . This yields the rate constant of  $[Ca^{2+}]_{in}$  decrease under Ca clamp of  $\approx 7.5 \cdot 10^{-4} s^{-1}$ . Maximum decrease rate constant obtained in one of 23 trials on 10 cells tested was  $3.3 \cdot 10^{-3} s^{-1}$ , whereas the average was  $(1.2 \pm 0.3) \cdot 10^{-3} s^{-1}$  (mean  $\pm$  SEM). In six trials, the average  $[Ca^{2+}]_{in}$  increase of  $(6.7 \pm 2.7) \cdot 10^{-4} s^{-1}$  rate was observed. Test of the clamp quality on steady backgrounds that closed 50–70% channels yielded the average  $(7.5 \pm 7.2) \cdot 10^{-4} s^{-1}$   $[Ca^{2+}]_{in}$  increase rate (four cells). Because the rate of  $[Ca^{2+}]_{in}$  turnover in amphibian rods bathed with normal Ringer is approximately  $1 s^{-1}$ , Ca clamping in our experiments retarded Ca feedback by at least 300-fold. Obviously, such a slow feedback cannot significantly affect sub-second flash responses considered further in this paper.

#### Determining the Time Course of PDE Activity

A long-time stay in the Ca-clamping solution was deteriorating to the cell. Therefore, we used the protocol that minimized cell exposure to the  $0 Na^+$ ,  $0 Ca^{2+}$  jet. It was as follows: recording rod saturated response (normal solution)  $\rightarrow$  recording averaged nonsaturated response (four to six trials, normal solution)  $\rightarrow$  recording single response to the same nonsaturating flash intensity (clamping solution)  $\rightarrow$  recording saturated response (clamping solution)  $\rightarrow$  return to normal solution. With this procedure, the time between the jump to the clamping solu-

tion and termination of the nonsaturated response did not exceed 15 s, and the total time in the clamping solution was not longer than 30 s per trial.

Fig. 3 A shows normalized nonsaturated current responses of a rod in a normal bath solution (curve 1) and after the jump into the jet of  $0 Na^+$ ,  $0 Ca^{2+}$  solution (curve 2). As expected, the trace in the Ca-clamping solution initially follows a normal response, but then reaches higher amplitude and lasts longer. After correcting for saturation,  $g_L = 4.8$  in this cell. Noisy line in Fig. 3 B shows the time course of the light-induced PDE activity,  $\beta_{fl}(t)$ , as derived from the curve 2 Fig. 3 A using Eqs. 3 and 5, and assuming  $n_{cG} = 3$ .

The ground for choosing this particular value for  $n_{cG}$  is explained in Fig. 4. Here, solid lines show a series of PDE responses to flashes of different intensities. The curves are calculated using  $n_{cG} = 3.0$  for the cooperativity of channel gating (see Eqs. 2, 3, and 5). Dashed lines show responses to two weaker flashes scaled up proportionally to the difference in intensity between them and the brightest flash. It is seen that the derived PDE responses scale linearly with the light intensity, as should be expected for the cascade that is far from saturation (see also Fig. 4 B, solid line). On the other hand, assuming  $n_{cG} = 2$  does not allow linear scaling (Fig. 4 B, dot-dashed line). In most cells, the test was not sensitive and only detected  $n_{cG}$  changes  $>0.5$ . Computations on five cells yielded the average  $n_{cG} = 3.2 \pm 0.3$ . Therefore, in Fig. 3 and for further analysis we accept the whole number  $n_{cG} = 3$ .

The simplest model of the PDE activation and inactivation predicts that the  $\beta_{fl}(t)$  curve is described with a difference of two exponentials:

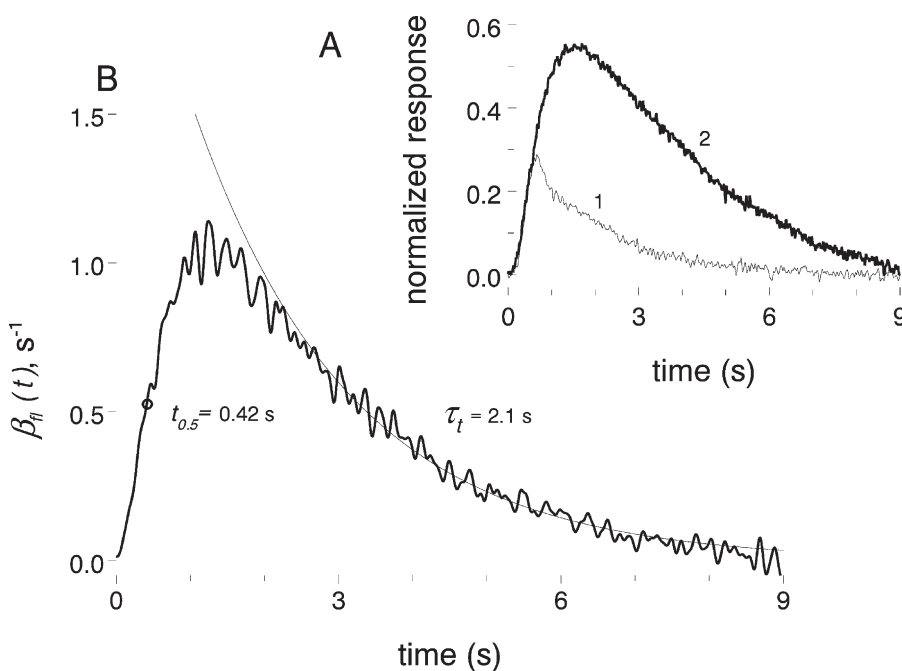


**Figure 3.** Finding flash-induced PDE activity from photoresponse recorded in  $Ca^{2+}$ -clamping solution. (A) Current responses of a rod to the same 10-ms, 13  $R^*$  flash applied in normal Ringer (curve 1, average of four responses) and in  $0 Na^+$ ,  $0 Ca^{2+}$  solution (curve 2, single response). Responses are normalized to the dark current level present before the flash. (B) The wave of flash-induced PDE activity (noisy curve) calculated from the curve 2 in A using Eqs. 3–5 in the text. Assumed:  $\beta_{dark} = 3.4 s^{-1}$ ,  $n_{cG} = 3$ . Smooth curve shows an exponential approximation of the recovery phase, starting from 60% maximum downward. Circle marks the half-height of the rising phase.

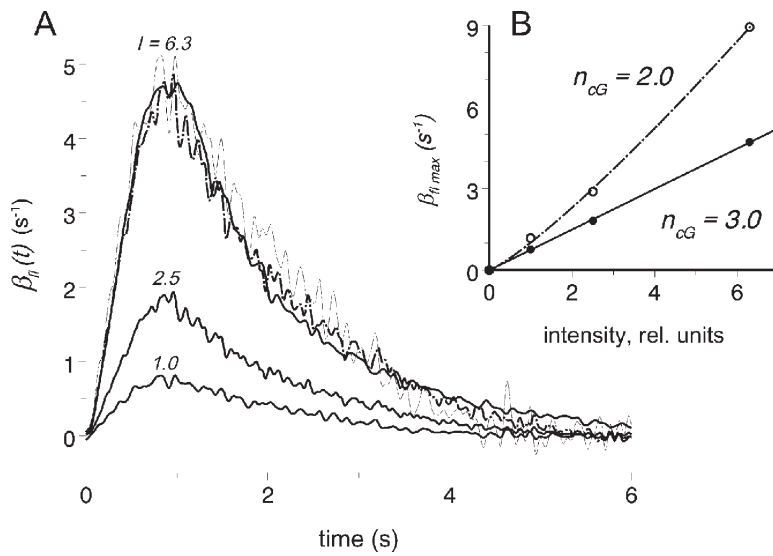


**Figure 4.** Intensity dependence of the PDE activity. (A) Series of PDE responses of the same cell to flashes of various intensities computed assuming  $n_{cG} = 3$  (solid lines). Numbers near the curves show relative intensities of the flashes. Relative intensity 1 = 10 R\*. Dashed lines are responses to weaker flashes scaled up to the brightest flash proportional to the intensity ratio. Trace I = 2.5 is average of three recordings; other traces, single recordings. (B, inset) Response versus intensity curves of the cell shown in A, plotted under assumption  $n_{cG} = 3$  (solid line through dots) or  $n_{cG} = 2$  (interrupted line through empty circles).  $n_{cG} = 3$  yields linear  $R$  versus  $I$  function, whereas that for  $n_{cG} = 2$  is nonlinear. Thus, the value  $n_{cG} = 3$  is accepted in all calculations.

$$\beta_R(t) = B \cdot (\exp(-(t - t_0)/\tau_1) - \exp(-(t - t_0)/\tau_2)), \quad (9)$$

where  $B$  is a proportionality factor,  $t_0$  is a delay, and  $\tau_1$ ,  $\tau_2$  are time constants of rhodopsin and transducin turn-off (e.g., Pugh and Lamb, 2000, Eq. 30). Formal two-exponential least-square fit to  $\beta_R(t)$  in Fig. 2 B yielded  $\tau_1 = 1.41$  s,  $\tau_2 = 1.28$  (fit not depicted). However, this sort of fitting to noisy experimental curves is not robust, especially if the two time constants lie close to each other. Therefore, we chose a more robust way to characterize the time courses of rising and falling phases of the PDE response. The decaying tail of the response, starting from 0.6 max downward, was fitted with a single exponential to determine its time constant  $\tau_t$  (Fig. 3 B, thin solid line). In most cases, this provided good quality fit with the coefficient of determination  $r \geq 0.95$ . The speed of the front was characterized by  $t_{0.5}$ , time at which the response reaches half of its peak value (Fig. 3 B, circle). Average values obtained on seven cells in dark adaptation are  $\tau_t = 1.8 \pm 0.2$  s (mean  $\pm$  SEM, range 1.25–2.6) and  $t_{0.5} = 0.48 \pm 0.06$  s (range 0.33–0.72).

It should be noticed that  $\tau_t$  and  $t_{0.5}$  do not allow a simple mechanistic interpretation. The entire time course of PDE activity is shaped by a combination of at least three quenching processes. Each of them affects, to a certain degree, the values of these parameters. Therefore, we use  $\tau_t$  and  $t_{0.5}$  just to characterize overall shape of the response and its changes during light adaptation (see below).

#### Effect of Background Illumination on the Kinetics of Cascade Shut-off

To study the effect of light adaptation on the PDE time course, we first registered Ca-clamped responses in the dark-adapted state following the protocol described above.

After returning the rod back to the normal Ringer, a steady background light was applied and the response was allowed to reach a steady level. Then, a saturating flash was delivered to probe the fraction of open channels. After recovery, the rod jumped into the Ca-clamping jet. A Ca-clamped response to a nonsaturating flash on steady background was recorded, and the saturating flash was repeated to determine the dark current value in this condition.

To calculate flash-induced  $\beta_R(t)$  on light background, steady pre-flash PDE activity  $\beta_0 = \beta_d + \beta_s$  should be substituted for  $\beta_d$  in Eq. 5. In principle, it could be possible to estimate  $\beta_0$  by jumps to IBMX, as described for  $\beta_d$ . We tested this approach and found that the effect of 0.5 mM IBMX on the cell was poorly reversible, which precluded further analysis of flash PDE responses on the same cell. Therefore, we relied on computational approach to estimate  $\beta_s$ .

Obviously,  $\beta_s$  depends on  $\beta_R(t)$ , and v.v. Assuming linearity of the PDE activation,

$$\beta_s = \frac{I_s}{I_{fl}} \int_0^\infty \beta_R(t) dt, \quad (10)$$

where  $I_{fl}$  is the intensity of the test flash (photons  $\cdot \mu\text{m}^{-2}$ ), and  $I_s$  is the background intensity (photons  $\cdot \mu\text{m}^{-2}\text{s}^{-1}$ ). Therefore, we started with a guess value of  $\beta_s$ , computed  $\beta_R(t)$  using Eq. 5, and then computed  $\beta_s$  from Eq. 10. Then, a new guess was made and the procedure was repeated until the two values for  $\beta_s$ , the guessed one and the one found from Eq. 10, coincided with sufficient accuracy, normally to three decimal digits.

Background light significantly accelerated the time course of the flash-induced PDE activity (Fig. 5 A). Remarkably, when flash responses in dark adaptation and on a steady background were normalized to flash intensity, light-adapted response returned to the pre-flash level

earlier, yet rising phases of the two responses coincided (Fig. 5 B). This means that light adaptation accelerated the turn-off process(es) but had no effect on cascade amplification. The conclusion is robust for the background intensities that blocked not more than  $\approx 50\%$  of the dark current. At stronger backgrounds, irregular variations of the circulating current in Ca clamp conditions resulted in large scatter of deduced  $\beta_{fl}(t)$  amplitudes among trials. However, the shape of the  $\beta_{fl}(t)$  curve at a given background was well-reproducible, so further conclusions regarding the effect of light adaptation on the turn-off kinetics are reliable.

It appeared that in many rods normalized light-adapted PDE responses could be made to virtually co-

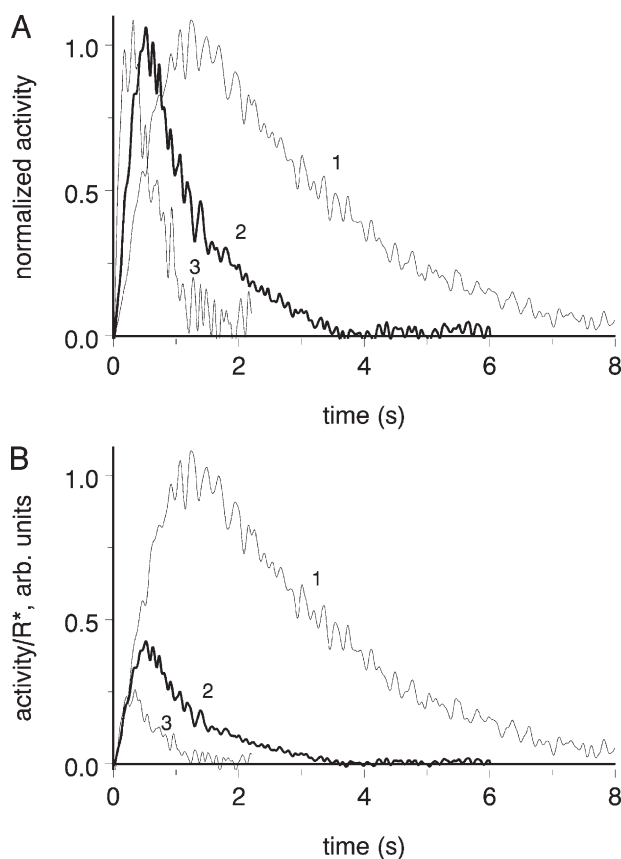


**Figure 5.** Effect of light adaptation on the time course and amplification of PDE activation. Same cell as in Fig. 3. (A) Flash-induced PDE response in dark adaptation (curve 1) and on the steady backgrounds that was applied before the jump into 0 Na<sup>+</sup>, 0 Ca<sup>2+</sup> solution and resulted in 27% (curve 2) and 42% (curve 3) suppression of the dark current. Responses are scaled to unity with respect to their peaks to more clearly show kinetic changes. Flash intensity 13 R\* (dark), 159 R\* (on background 170 R\*s<sup>-1</sup>), and 82 R\* (on background 490 R\*s<sup>-1</sup>). Background-induced steady PDE activity ( $\beta_s$ ) is 2.7 s<sup>-1</sup> on weaker and 3.6 s<sup>-1</sup> on brighter background. (B) Same responses as in A, but the responses on background, instead of normalization to unity, are scaled down inversely proportional to the ratio of flash intensities. Fronts of the three curves virtually coincide, showing that the rate of activation of the cascade (amplification) is not affected by light adaptation.

incide with the dark response by a simple expansion along the time axis (Fig. 6 A). This suggests that both shut-off processes shaping the response are under light-adaptation control and are accelerated by background light to approximately the same extent. In the rod shown in Fig. 6, the background that reduced circulating current by 27% resulted in a 2.5-fold acceleration of the entire  $\beta_{fl}(t)$  curve. The background light that closed 42% of the channels produced an  $\approx 4.6$ -fold acceleration.

However, in half of rods time scaling did not work, that is, the time courses of the front and the tail were differently affected by light adaptation. Therefore, to quantitatively characterize the background-induced acceleration, we used the analysis depicted in Fig. 3 B. It confirmed the results obtained with plain time scaling like in Fig. 6 A. Plotting  $\beta_{fl}(t)$  on log scale transforms the exponential tail of the response into a long linear stretch

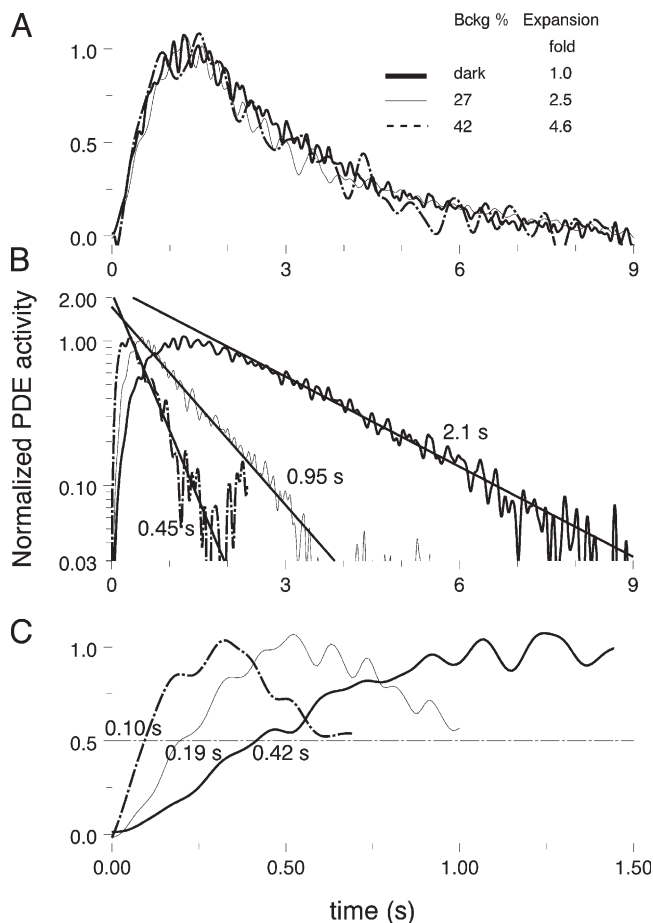


**Figure 6.** Light adaptation shortens both the rising and falling phases of flash PDE response. Same cell as in Figs. 3 and 5. (A) In this and many other cells, responses on backgrounds of varying intensity can be made to coincide with the dark-adapted response by proper expansion along the time axis. Legend near the curves shows the fraction of dark current blocked by the background, and corresponding expansion factor. (B) Curves from A plotted on log scale against common time axis. Solid straight lines show exponential approximation of the recovery phase. (C) Fronts of the curves from A, with circles marking half-rising time  $t_{0.5}$ .



whose slope increases with increasing background intensity (Fig. 6 B). The front of the response, as characterized by  $t_{0.5}$ , also gets faster (Fig. 6 C). Acceleration of the tail by backgrounds closing 27 and 42% channels of the dark current was 2.2- and 4.7-fold, respectively. Fronts were shortened by 2.2- and 4.2-fold, in reasonable agreement with the values obtained with the time scaling of the responses (Fig. 6 A).

There was a big scatter among cells with respect to steepness and magnitude of background-induced acceleration of turn-offs (Fig. 7, A and B). Acceleration is plotted versus fold dark current suppression  $I_d/I_b$ , which is supposed to reflect the decline in the intracellular free  $\text{Ca}^{2+}$  level (Gray-Keller and Detwiler, 1994, 1996; Younger et al., 1996). Maximum acceleration of the tail was 5.5-fold at 58% (2.4-fold) dark current suppression (Fig. 7 A, the cell labeled by open diamonds). Maximum shortening of the front was 7.6-fold at 69% (3.2-

fold) dark current suppression (Fig. 7 B, the cell labeled by filled triangles). By linear interpolation between data points for individual cells, we calculated an average acceleration versus dark current suppression functions (Fig. 7 C, filled and empty circles). To approximate front and tail acceleration data, we used a Hill-type equation:

$$a(f) = \frac{a_{\max} \cdot (kf)^h}{1 + (kf)^h}, \quad (11)$$

where  $a(f)$  is the acceleration factor,  $f = I_d/I_b$ ,  $k$  is a scaling constant,  $h$  is the Hill coefficient, and  $a_{\max} = 1 + 1/k^h$ . The function is forced to pass through (1, 1) point. The least-square fit yields  $a_{\max} = 3.6$ ,  $h = 5.2$ ,  $k = 0.83$  for  $\tau_t$ , and  $a_{\max} = 5$ ,  $h = 5.8$ ,  $k = 0.79$  for  $t_{0.5}$ . However, the steepest initial part of the curves can be fitted by  $a(f) = f^h$ , with  $h = 2.5$ –3.

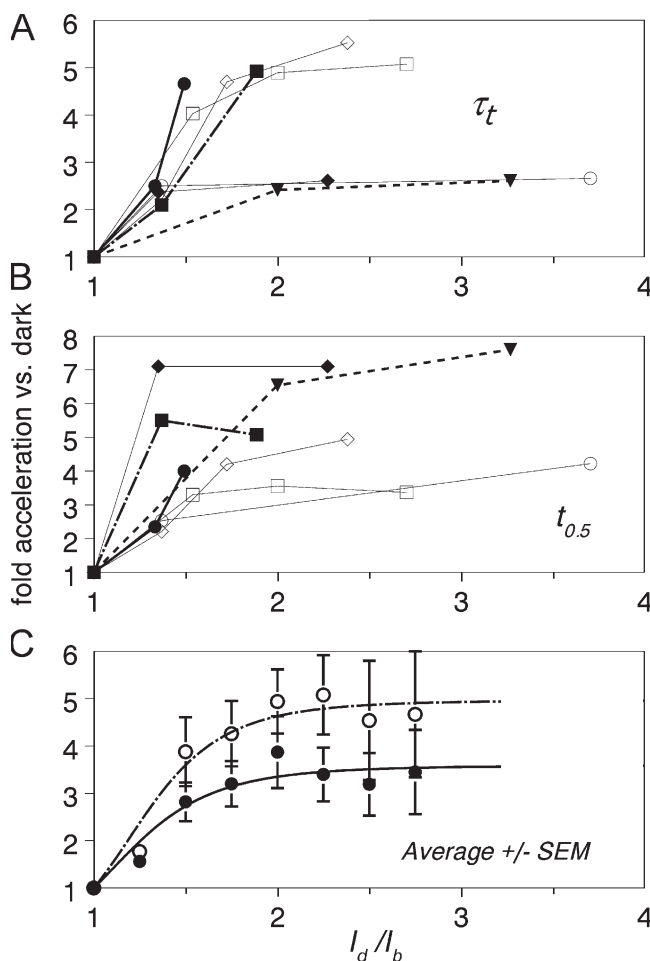


**Figure 7.** Dependence of the acceleration of the cascade shut-off on the dark current suppression by background. Data for individual cells are shown by different symbols/line styles. (A) Time constant of the recovery phase  $\tau_t$ . (B) Half-rising time  $t_{0.5}$ . (C) Average  $\pm$  SEM obtained by interpolation between experimental points. Filled circles,  $\tau_t$ ; empty circles,  $t_{0.5}$ . Smooth curves show Hill-like approximations (Eq. 11) with the parameters given in the text.

#### Dominant Shut-off Time Constant Is Independent of Light Adaptation

The dominant shut-off time constant  $\tau_D$  has previously been tentatively identified with transducin/PDE shut-off time constant  $\tau_E$  in salamander (Lyubarsky et al., 1996; Nikonov et al., 2000). The conclusion was based on independence of  $\tau_D$  from background light that would accelerate rhodopsin phosphorylation via  $\text{Ca}^{2+}$  feedback and thus reduce  $\tau_R$ . We confirm background invariance of  $\tau_D$  in *R. ridibunda* rods (Fig. 8). For example, in the cell shown in Fig. 8, the background illumination that closed 72% light-sensitive channels and accelerated the recovery from saturation by  $\approx 7$  s had no significant impact on the slope of the Pepperberg line. The same result was obtained in all rods tested (six cells) at background intensities blocking from 30 to 75% of the dark current.

On average,  $\tau_D$  in the same group of cells that was used to obtain  $\tau_t$  and  $t_{0.5}$  in the dark-adapted state (see above) did not differ significantly from the time constant of the tail of the PDE response ( $1.74 \pm 0.21$  s vs.  $1.8 \pm 0.2$  s, respectively). Yet, as shown earlier, background illumination shortened both the tail and the front of the PDE response by over fivefold (compare with Fig. 7) without having any effect on  $\tau_D$ . This suggests that  $\tau_D$  does not characterize the main phase of either rhodopsin or transducin shut-offs in the frog, at least in the light-adapted state.

#### Desensitization Revealed by the Saturation Time Analysis Is Not Due To Reduced Amplification

The horizontal shift of the Pepperberg line induced by steady backgrounds characterizes desensitization due to light adaptation. On average, the background light that resulted in closure of 50% of the light-sensitive channels produced  $41 \pm 17$ -fold desensitization (four cells, mean  $\pm$  SEM). Maximum desensitization observed was

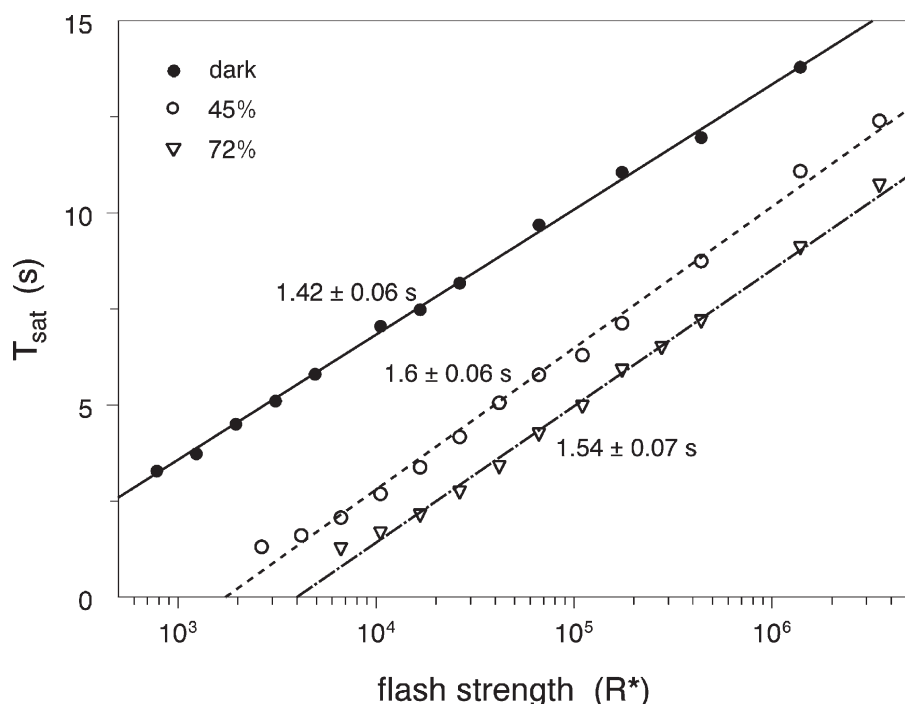


**Figure 8.** Independence of the dominant time constant of the cascade quenching from light adaptation. Saturation time versus flash intensity functions are shown for a dark-adapted rod and at two backgrounds of different intensities. Each point in dark-adapted state and at 45% background is the average of two recordings. Four recordings are averaged at brighter (72%) background. Recovery from saturation is taken as the moment of regaining 1.5 pA ROS current, which is equal to 10% dark current. Straight lines are least-square fits to data with Eq. 7; three initial points on the shallow part of the background curves are excluded from fitting. Numbers near the lines show  $\tau_D$  values derived from the fit (mean  $\pm$  SEM).

85-fold at the background that closed 55% dark current channels. To test whether the decrease of amplification within the cascade contributes to desensitization, we determined the amplification by fitting the rising phases of normalized saturated responses by

$$r(t)/r_{\max} = 1 - \exp(-\frac{1}{2}A \cdot R^* \cdot (t - t_0)^2), \quad (12)$$

where  $t$  is time,  $t_0$  is the transduction delay,  $R^*$  is the flash intensity expressed in the number of activated rhodopsins, and  $A$  is the amplification (Pugh and Lamb, 2000).

An example of the fit is given in the inset in Fig. 9. Symbols show the front of the response to  $\approx 3,000 R^*$  in dark adaptation (solid dots) and on 50% background (circles), of the cell whose  $T_{\text{sat}}$  versus  $I$  functions are plotted in Fig. 8. Smooth lines are fits to each set of data with Eq. 12. No change in the cascade amplification is seen.

The (apparent) cascade amplification extracted from this analysis is intensity dependent because the slope of the response ( $1/2A \cdot R^*$  in Eq. 12) is not strictly proportional to  $R^*$  but rather tends to saturate at bright flashes. Similar saturation of the slope has been observed in

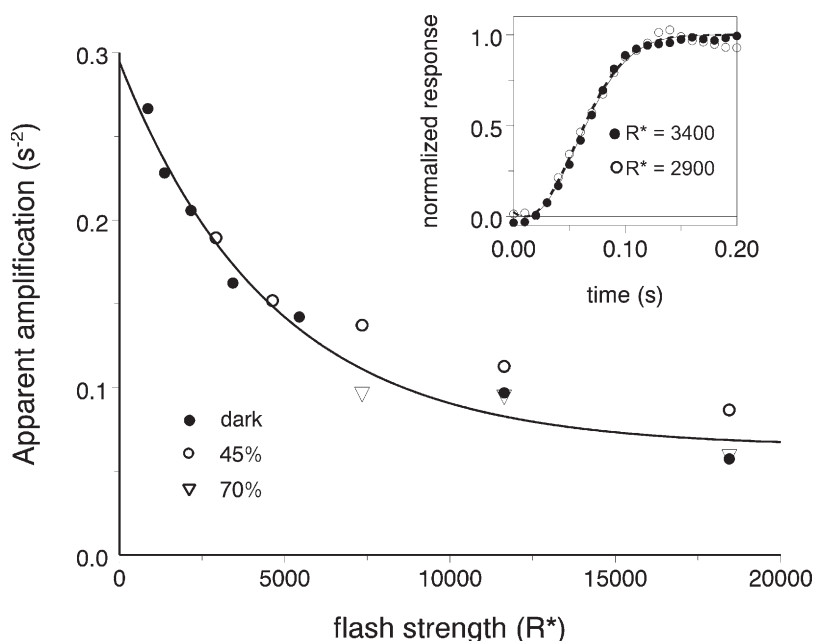


**Figure 9.** Light adaptation does not affect the cascade amplification. Inset shows fronts of two current responses to saturating flashes of nearly identical intensities (filled circles, dark adaptation; open circles, background blocking 45% of the dark current). Smooth lines are fits to the data with Eq. 12. No reduction of amplification by light adaptation is seen. Main panel shows the apparent amplification constant ( $A$  in Eq. 12) as a function of the flash strength and adaptation state. Smooth exponential line is drawn to visually connect the points and bears no mechanistic meaning. Same cell as in Fig. 8.

salamander (Lamb and Pugh, 1992) and human rods (Smith and Lamb, 1997). The saturation in frog is incipient at flash intensities an order of magnitude lower than in salamander. This is in a general agreement with higher sensitivity of frog rods (amplification constant of  $\approx 0.3 \text{ s}^{-1}$  compared with  $0.07 \text{ s}^{-1}$  in salamander). An additional factor contributing to the difference may be that Lamb and Pugh (1992) made recordings in voltage-clamp condition that eliminates the low-pass filter effect of the cell's electrical time constant. Suction pipette and ERG recordings are influenced by the filtering (Smith and Lamb, 1997).

Our unpublished data suggest that the electrical filtering is not a complete explanation in our experiments. However, the analysis of the cause(s) of the saturation is beyond the scope of the present work. Therefore, we measured the amplification with flashes of various intensities applied in dark and on adapting backgrounds, and found no evidence of amplification reduction during light adaptation, at background lights that shut up to 75% of the dark current (Fig. 9, main panel).

## DISCUSSION

The approach to extracting the time course of the light-induced PDE activity from the  $\text{Ca}^{2+}$ -clamped response was suggested by Rieke and Baylor (1998). We used it to characterize flash-induced PDE activity and to study the effect of light adaptation on the kinetics of turn-off of phototransduction cascade in frog rods.

### Amplification in the Ca Feedback Loop and the Efficiency of $[\text{Ca}^{2+}]_{\text{in}}$ Clamping

Because the constancy of  $\alpha_d$  is a prerequisite to our analysis, the stability of  $[\text{Ca}^{2+}]_{\text{in}}$  under clamp conditions had to be tested. Efficiency of the Ca-clamping procedure was assessed from its effect on the time integral of flash responses and from the stability of the dark current in 0  $\text{Ca}^{2+}$ , 0  $\text{Na}^+$  solution. It appeared that the average rate of  $[\text{Ca}^{2+}]_{\text{in}}$  changes in 0  $\text{Ca}^{2+}$ , 0  $\text{Na}^+$  solution is more than two orders of magnitude slower than changes that shape photoresponses in normal Ringer. Possible uncertainty of the procedure of correction for response saturation cannot invalidate this estimate.

One can argue that the stability of dark  $[\text{Ca}^{2+}]_{\text{in}}$  in the clamping solution does not guarantee its constancy during flash responses. However, free  $\text{Ca}^{2+}$  level in the clamping solution is in nanomolar range, so both passive  $\text{Ca}^{2+}$  fluxes through the light-sensitive channels and active efflux via the exchanger are greatly diminished compared with their values in normal Ringer. Therefore, possible misbalance of the fluxes due to the transient closure of the channels cannot substantially affect  $[\text{Ca}^{2+}]_{\text{in}}$ . The fluorescence data of Matthews and Fain (2001) support this notion. The authors show that instantaneous complete closure of the light-sensitive channels in a salamander

rod bathed in Ca-clamping solution results in the  $[\text{Ca}^{2+}]_{\text{in}}$  decline with the time constant of  $\approx 100 \text{ s}$ . This is over two orders of magnitude slower than characteristic times of light-adapted responses that lie in a sub-second range (our Figs. 5, 6, and 10).

We conclude that greatly retarded residual calcium feedback cannot noticeably affect the deduced PDE waveform and account for its acceleration by light adaptation.

### Both Rhodopsin and Transducin Shut-offs Are under Light Control

Perhaps the most unexpected result of this study is that a nonsaturating background illumination significantly accelerates both the shut-off processes that shape the main phase of flash-induced PDE activity (Figs. 5 and 6). It is worth noting that neither of the two characteristic times of  $\beta_{fl}(t)$  extracted by our analysis can be unambiguously attributed to rhodopsin or transducin shut-offs. It is always the slower process that mainly shapes the falling tail of the response, and the faster one that shapes the front.

Furthermore, reduction of  $t_{0.5}$  partly results from the acceleration of  $\tau_r$ . This is because an acceleration of the decay phase reduces the amplitude of the response, so it takes less time to reach the half-peak value. Bigger range of regulation of  $t_{0.5}$  as compared with  $\tau_t$  (Fig. 7 C, open vs. filled circles) should, at least partly, be attributed to this fact. However, shortened  $\tau_t$  (and decreased response amplitude caused by it) is not the sole factor responsible for abbreviated front. Because the tail of the response is significantly slower than its front (compare average  $\tau_t$  and  $t_{0.5}$  values), reduction of  $\tau_t$  as such would have a relatively small effect on the response amplitude and hence on  $t_{0.5}$ . For instance, the modeling described in Discussion and Appendix suggests that a 4.2-fold shortening of  $t_{0.5}$  by the brighter background seen in Figs. 5, 6, and 10 is caused by a 3.3-fold acceleration of the faster turn-off process.

We conclude that both processes, the faster one that mostly shapes the front of the flash PDE response and the slower one mainly responsible for its decay phase, are under light-adaptation control.

It is generally believed that the slower phase is controlled by transducin quenching. Thus, Lyubarsky et al. (1996) found in salamander that the time constant of the tail of the current response, roughly 2 s, is background independent and equal to  $\tau_D$ . Because rhodopsin quenching by phosphorylation is under calcium/light-adaptation control via recoverin, the authors concluded that it is transducin turn-off that is the slower process. Further, by modeling the entire flash response in  $\text{Ca}^{2+}$ -clamping solution, Lyubarsky et al. (1996) found that the time constant of the faster process (that is, of rhodopsin phosphorylation) is approximately 0.4 s in the dark-adapted state. Sagoo and Lagnado (1997) reached a similar conclusion. The identity of  $\tau_D$  with  $\tau_E$  in mouse

has been definitely shown by Krispel et al. (2006) who found that varying the expression level of the RGS9 complex changes in a concerted way both  $\tau_D$  and the decay phase of the response. Overexpression of the GAP complex can reduce both the time constants to  $\approx 80$  ms (compared with  $\approx 200$  ms in wild-type mice), which sets the upper limit for  $\tau_R$ . Finally, various mathematical models of phototransduction can satisfactorily reproduce photoresponses under the assumption that  $\tau_E = \tau_D > \tau_R$  (Nikonov et al., 2000; Hamer, 2000a, 2000b; Hamer et al., 2003, 2005). This also holds for *R. ridibunda* rods used in the present study (Kuzmin et al., 2004).

If one assumes that transducin turns off slower than rhodopsin in frog rods, our results directly show that the transducin quenching can be substantially accelerated by light adaptation (Figs. 6 B and 7 A). If, to the contrary,  $\tau_E < \tau_R$  in *R. ridibunda* (that is, transducin turn-off is mainly responsible for the front of the PDE response), one can see that the light adaptation accelerates the process that shapes the rising phase of  $\beta_{fl}(t)$  as well (Figs. 6 A and 7 C). Thus, regardless of what is which, light adaptation has a profound effect on both turn-off processes that shape the main phase of the PDE response.

One could argue that there is the third process that also contributes substantially to shaping the waveform of the PDE activity, namely arrestin binding to phosphorylated rhodopsin. Then, an accelerated (by whatever mechanism) arrestin binding could possibly explain faster recovery of the light-adapted response. A priori this does not seem probable because arrestin binding is

only responsible for a slow quenching of a low-amplitude tail of rhodopsin catalytic activity, as follows from all biochemical data and is supported by the results on arrestin knockout mice (Xu et al., 1997; see also the model by Hamer et al., 2003, their Fig. 5). However, to test this possibility, we created a simple mathematical model of the cascade turn-off that explicitly considers two-step quenching of photoactivated rhodopsin. The model is described in the Appendix. It does not include a detailed treatment of sequential phosphorylation of rhodopsin, like in elaborated models by Hamer et al. (2003, 2005). Because a dozen of parameters that are necessary for a detailed model are not known, we assume for simplicity a single-exponential partial quenching of rhodopsin by phosphorylation that is followed by a single-exponential binding to arrestin. Rhodopsin phosphorylation is characterized by the time constant  $\tau_R$ , and arrestin binding is characterized by the time constant  $\tau_A$ . Two other parameters that shape the PDE response are  $\tau_E$ , time constant of transducin turn-off, and  $a < 1$ , fractional (with respect to fully active metarhodopsin II) activity of phosphorylated yet arrestin-unbound rhodopsin. The magnitude of the PDE wave is proportional to  $R^* \cdot A$ , the product of flash intensity and cascade amplification.

Fig. 10 shows the result of modeling of the PDE responses of the cell used to plot Figs. 3, 5, and 6. To restrict the freedom of parameters, we chose  $a = 0.09$  and  $\tau_A = 1.6$  s, as follows from our further analysis and the Pepperberg plot for this cell (see two next sections and Fig. 10). Three remaining parameters, namely  $\tau_R$ ,  $\tau_E$ , and

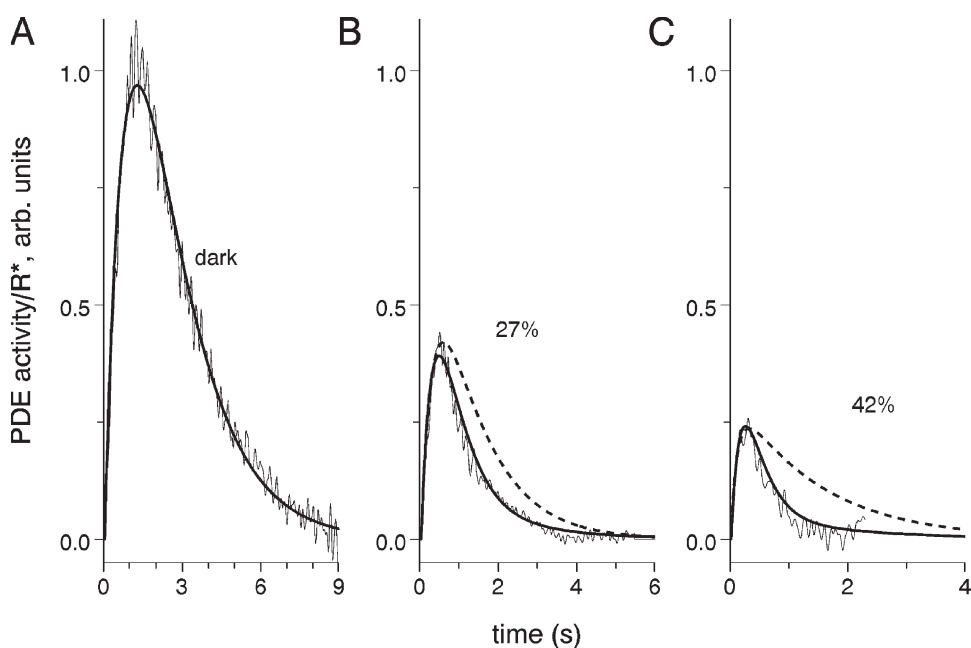


**Figure 10.** Modeling  $PDE(t)$  waveform with the three-stage quenching model described in the Appendix. Experimental responses from Fig. 5 B are fitted with Eqs. 3a–6a. Smooth solid lines show least-square fits obtained with the MathCad genfit procedure. Fractional activity of phosphorylated yet arrestin-unbound rhodopsin is fixed at  $a = 0.09$ .  $\tau_A = 1.6$  s follows from Pepperberg-type analysis on this cell. Free parameters are  $\tau_R$ ,  $\tau_E$ , and the product of  $R^* \cdot \nu_{RE} \cdot \beta_{sub}$  that determines the response amplitude. The fits yield  $\tau_R = 0.96$  s and  $\tau_E = 1.44$  s in the dark-adapted state (A). Corresponding values in light adaptation are 0.47, 0.39 s (background blocking 27% dark current, B), and 0.29, 0.18 s (42% blockade, C). Dashed lines show the fits obtained by manually varying  $\tau_R$  and  $\tau_A$  while keeping  $\tau_E = 1.44$  s at its dark-adapted level. The rising phase of the light-adapted response can only be fitted.



magnitude of the response, were found by least-square fit of experimental  $PDE(t)$  curves with Eqs. 3a–6a using the genfit procedure in MathCad. Fit was robust in the sense that varying initial guessed values within an order of magnitude range yielded the fits that converged to virtually the same parameters. The model provides a good description of the PDE response in the dark-adapted state (Fig. 10 A, bold smooth line). Automatic fits to the light-adapted responses result in the shortening of  $\tau_R$  and  $\tau_E$  while keeping  $a$  and  $\tau_A$  constant (Fig. 10, B and C, smooth solid lines; parameters of the fits are given in the figure legend). Notably, the amplification  $A$  obtained from the fit also remained unchanged within <15%.

On the other hand, it appeared impossible to mimic the effect of light adaptation by allowing  $\tau_R$ ,  $\tau_A$  acceleration and keeping  $\tau_E$  at its dark-adapted value. Formal least-square fits generated the curves that grossly deviated from the experiment (fits not depicted). It was possible to obtain a good fit of the rising phase by manually adjusting  $\tau_R$  and  $\tau_A$ , but the recovery phases of the model and experimental responses were in strong disagreement (Fig. 10, B and C, heavy dashed lines).

Thus, modeling shows that speeded arrestin binding cannot explain the acceleration of the PDE recovery phase. On the other hand, accelerating both  $\tau_R$  and  $\tau_E$  reproduces all salient features of the effect of light adaptation on the PDE response. This supports the idea that not only rhodopsin but also transducin quenching is under light-adaptation control.

An important result of modeling is that the formal analysis of the decaying phase of the response depicted in Figs. 6 and 7 may underestimate the extent of regulation of the underlying shut-off process(es). Thus,  $\approx 4.5$ -fold acceleration of the recovery phase in the cell shown in Fig. 6 is reproduced in the model by an approximately eightfold acceleration of  $\tau_E$  (see legend to Fig. 10).

To our knowledge, there are two works in which an effect of light adaptation on transducin shut-off was detected. Krispel et al. (2003) found in mouse rods that the saturation time and  $\tau_D$  (which in mouse represents  $\tau_E$ ) decreased after 3 min of bright saturating illumination, without noticeable change in the amplification constant. The effect was seen after complete recovery of the dark current and disappeared in darkness in a couple of minutes. Reduction of  $\tau_i$  and  $\tau_D$  during steady light adaptation in mice rods was also described by Woodruff et al. (2008), although the magnitude of the effect was substantially smaller than that found by Krispel et al. (2003).

There is a notable difference between the effects discovered in mice and the acceleration of transducin shut-off found by us in the frog. In mice, the biggest acceleration observed as an after effect of bright flashes is approximately twofold (Krispel et al., 2003). The reduction of  $\tau_E$  in our experiments on frog rods occurs on steady nonsaturating backgrounds and is substantially larger, more than eightfold.

Apparently, there is no firmly established mechanism(s) by which light adaptation could regulate the lifetime of activated transducin. A possible target for the regulation might be RGS9-1. It is known that RGS9-1 is phosphorylated in vivo in dark-adapted rods with a photoreceptor-specific protein kinase C, and that the phosphorylation level reduces in light (Hu et al., 2001; Wensel, 2002; Sokal et al., 2003). cAMP-dependent protein kinase A may also contribute to light-dependent phosphorylation (Balasubramanian et al., 2001). Yet functional effects of changing phosphorylation level are unclear. Balasubramanian et al. (2001) found that in vitro the GAP activity of RGS9 is reduced by its phosphorylation. Thus, high  $\text{Ca}^{2+}$  and cAMP levels characteristic of the dark-adapted state may keep RGS9 phosphorylated and transducin turn-off rather slow. Decrease in  $[\text{Ca}^{2+}]_{\text{in}}$  or  $[\text{cAMP}]$  by background light would then accelerate the shut-off. However, magnitude of the regulatory effect in vitro is quite modest compared with the acceleration revealed in our experiments. Besides, it is reported that cAMP has no effect on the photoresponse of truncated gecko “rod” outer segments (Jindrova and Detwiler, 2000). So it remains to be seen whether the adaptation-dependent phosphorylation of RGS9 can explain the acceleration of transducin quenching observed in physiological experiments.

#### Dominant Turn-off Time Constant $\tau_D$ Is Not That of Either Rhodopsin Phosphorylation or Transducin Quenching in the Frog Rods

Originally,  $\tau_D$  has been attributed to  $\tau_R$ , the time constant of rhodopsin quenching (Pepperberg et al., 1992). Later it was identified with  $\tau_E$ , the time constant of transducin turn-off (Lyubarsky et al., 1996; Nikonov et al., 2000; Krispel et al., 2006). However, the idea that the PDE time course is shaped by two first-order reactions, those of rhodopsin phosphorylation and GTP hydrolysis by transducin, is a clear oversimplification. A controversy about the source of reproducibility of the single-photon response (Rieke and Baylor, 1998; Whitlock and Lamb, 1999) led finally to the conclusion that rhodopsin turn-off depends on multiple serial phosphorylation events (Field and Rieke, 2002; Hamer et al., 2003, 2005; Doan et al., 2006). This only approximately results in a single-exponential decay of activity (Hamer et al., 2003). Besides, quenching by phosphorylation is incomplete, and further turn-off relies on capping phosphorylated rhodopsin with arrestin (Wilden et al., 1986; Bennett and Sitaramayya, 1988; Palczewski et al., 1992; Xu et al., 1997; Vishnivetskiy et al., 2007). Then, quenching proceeds during the decay of phosphorylated and arrestin-bound metarhodopsins to retinal and opsin, and is only complete after regeneration of dark visual pigment. Thus, the Pepperberg plot is not straight at all, and can only be approximated by a series of (roughly) straight stretches, each controlled by a different dominant process (Firsov et al., 2005).

The Pepperberg analysis is usually applied to the initial part of the  $T_{sat}$  versus  $\ln(Intensity)$  plot, for saturation times roughly between 2 and 20 s in amphibian rods (compare with Fig. 8). Then the question is, What process underlies this phase of recovery from saturation? It is clearly not the main phase of either rhodopsin or transducin shut-offs that result in quenching of nonsaturating responses in the frog rod. First, we show that both rising and decaying phases of the response are under light-adaptation control (Fig. 6), whereas  $\tau_D$  is adaptation independent (Fig. 8). Second, the characteristic times of PDE response in light-adapted conditions are markedly faster than  $\tau_D$ , and the difference may be almost 10-fold (Fig. 6).

One may tentatively attribute  $\tau_D$  to the time constant of arrestin binding to rhodopsin partially quenched by phosphorylation. This means that the main phase of the cascade inactivation is controlled by rhodopsin phosphorylation and transducin/PDE shut-off. The two main processes shape the waveform of the photoresponse to nonsaturating stimuli. Arrestin binding is then responsible for a low-amplitude slow tail of the response that hardly can be revealed by routine curve fitting of noisy experimental recordings, as clearly seen from detailed mathematical modeling (Hamer et al., 2003, 2005). However, at bright flashes the main phase of quenching is complete while the cell still stays in saturation, so it is arrestin binding that now controls the recovery time. The process is believed to be  $Ca^{2+}$  independent, which would explain the constant slope of the  $T_{sat}$  versus  $\ln(Intensity)$  plot regardless of the adaptation state (Fig. 8). A mathe-

matical model based on this assumption provides a good description of the Pepperberg plot in dark adaptation and on light backgrounds (Fig. 11; see Appendix and the next section).

The conclusion about the process responsible for the initial part of the  $T_{sat}$  versus  $\ln(Intensity)$  function may be species and adaptation specific. For example, in salamander it may be transducin quenching, as suggested by Lyubarsky et al. (1996), Sagoo and Lagnado (1997), and Nikonov et al. (1998). It may also be true of mouse rods (Krispel et al., 2003, 2006). This depends on which of the three main quenching processes, namely rhodopsin phosphorylation, arrestin binding, and transducin GTP-ase, is the slowest in a given animal in the given adaptation state.

#### The Accelerated Shut-offs Can Account for Desensitization by Light Adaptation

The rightward shift of the  $T_{sat}$  versus  $\ln(Intensity)$  plot during light adaptation can be interpreted as a sensitivity reduction (Fig. 8). Noticeably, in the frog the desensitization may reach 85-fold. This is significantly larger than that found with a similar paradigm in the salamander (approximately fourfold, Pepperberg et al., 1992; approximately 10-fold, Nikonov et al., 2000), toad (11-fold, Murnick and Lamb, 1996), or mouse (approximately fourfold; Krispel et al., 2006). The desensitization determined this way is usually interpreted in terms of Eq. 7. Within this framework, rightward shift of the  $T_{sat}$  versus  $\ln(I)$  function during light adaptation can be attributed to either an increase of  $C$  or a reduction of gain  $g$ . In their

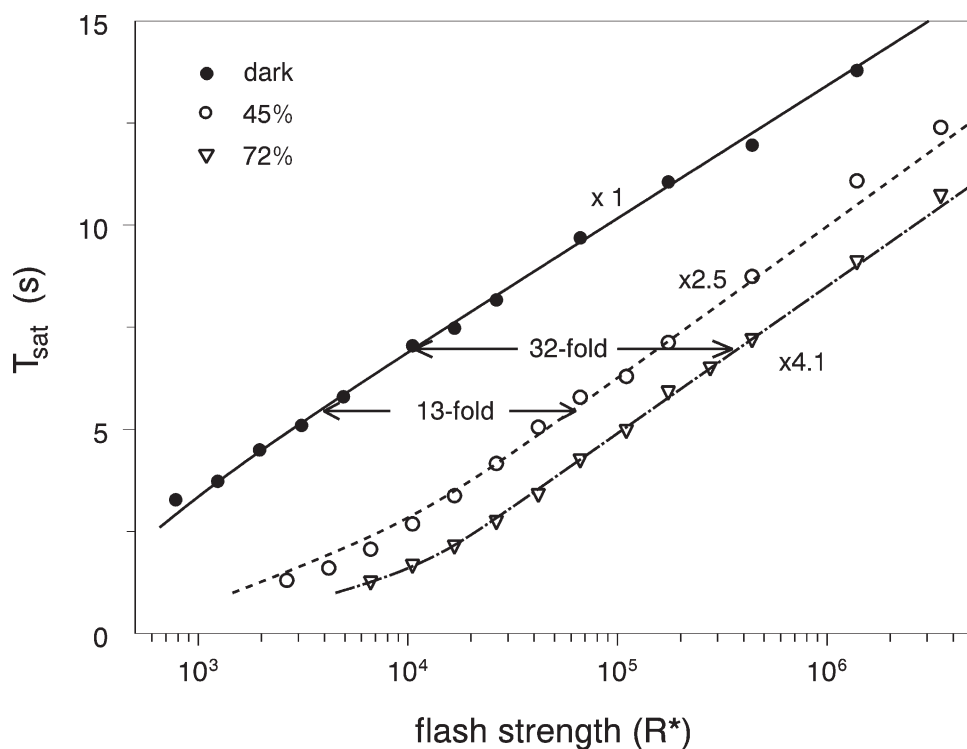


**Figure 11.** Modeling the sensitivity reduction by light adaptation with accelerated cascade shut-offs. Experimental data from the same cell as in Figs. 8 and 9. Fold sensitivity reduction is defined as the shift of the Pepperberg plot along the intensity axis. Smooth lines are predictions of the three-stage quenching model described in the Appendix, with parameters given in the main text. Concurrent acceleration of rhodopsin phosphorylation and transducin shut-off is sufficient to reproduce experimental data fairly well. Acceleration factors are given near the curves.

first paper, Pepperberg et al. (1992) apparently favored the former explanation. Later, they postulated the gain decrease.  $\tau_D$  was identified with  $\tau_R$ , the time constant of rhodopsin turn-off by phosphorylation, and the site of the gain decrease was placed either at the stage of transducin activation by rhodopsin or at transducin inactivation (Pepperberg et al., 1994; Pepperberg, 2001).

However, if the recovery-controlling substance (say,  $T^*/PDE^*$ ) is produced by light via an intermediate (say,  $R^*$ ), the apparent gain becomes dependent on the lifetime of the intermediate. For instance, in case of a single-exponential quenching of  $R^*$  and  $T^*$ , the flash-evoked hydrolytic activity of  $PDE^*$  is given by

$$P^*(t) = \frac{\tau_R \tau_E \cdot \nu_{RE} \beta_{sub} \cdot I}{\tau_E - \tau_R} (\exp(-t/\tau_E) - \exp(-t/\tau_R)), \quad (13)$$

where  $\tau_R$  is the time constant of rhodopsin phosphorylation,  $\tau_E$  is the time constant of transducin quenching,  $\nu_{RE}$  is the rate of transducin activation by fully active  $R^*$ , and  $\beta_{sub}$  is the catalytic activity of the PDE subunit (Appendix, Eq. 3a; compare with Pugh and Lamb, 2000, Eq. 30). It is evident that the magnitude of  $P^*(t)$  depends not only on  $\nu_{RE} \cdot \beta_{sub}$  (amplification), but also on  $\tau_R$  and  $\tau_E$ .

Thus, the gain changes revealed by the analysis of the  $T_{sat}$  versus  $\ln(Intensity)$  function may include two components. One represents true biochemical amplification  $\nu_{RE} \cdot \beta_{sub}$  which characterizes the initial rate of activation of the cascade. The other one is a function of lifetimes of active intermediates (see discussion between Pepperberg [2001] and Nikonov et al. [2001]). In accordance with earlier data (Nikonov et al., 2000; Krispel et al., 2003), we show here that the light adaptation has no effect on the rate of activation of the cascade ( $\nu_{RE} \cdot \beta_{sub}$  = amplification in Pugh and Lamb, 2000 sense; Figs. 5 and 9). However, it results in a drastic decrease of the gain measured in Pepperberg-type experiments. This should be attributed to a corresponding reduction of  $\tau_R$  and/or  $\tau_E$ .

As argued above, neither  $\tau_R$  nor  $\tau_E$  represents  $\tau_D$ , the adaptation-invariant rate of the process that controls recovery from saturating flashes. We tentatively identified it with the time constant of arrestin binding to  $R^*$  partially inactivated by phosphorylation ( $R_p$ ). Hence, the kinetic model that would account for our experimental findings should include three active components, namely  $R^*$ ,  $R_p$ , and  $T^*/PDE^*$ . Derivation of corresponding equations that describe the time courses of concentrations of  $R^*$ ,  $R_p$ , and  $T^*/PDE^*$  is given in the Appendix.

The results of modeling of  $T_{sat}$  versus  $I$  curves for the cell shown in Fig. 8 are illustrated in Fig. 11. For the dark-adapted state, values of  $\tau_E = 1.25$  s and  $\tau_R = 0.9$  s were chosen within the range obtained experimentally on an independent group of cells. The value of  $\tau_A = 1.6$  s corresponds to  $\tau_D$  found in this cell. Fractional activity

of phosphorylated yet arrestin-unbound rhodopsin  $a = 0.09$  was chosen to obtain a good fit to experimental data. The amplification and criterion level  $C$  were adjusted to ensure the right position of the model curve with respect to the intensity axis (Fig. 11, solid line through filled circles).

To mimic the effect of light adaptation,  $\tau_E$  and  $\tau_R$  were concurrently reduced to achieve a good fit to the  $T_{sat}$  versus  $\ln(I)$  relationships in two light-adapted states. It appeared that the 13-fold desensitization induced by the background that closed 45% dark channels could be reproduced by a 2.5-fold acceleration of both rhodopsin phosphorylation and transducin shut-off (Fig. 11, dashed line through empty circles). The 32-fold desensitization at 72% background is produced by a 4.1-fold acceleration of both the processes (Fig. 11, dot-dashed line through triangles). Notably, keeping  $\tau_A = \tau_D$  provides an excellent fit to all three sets of data, thus supporting the idea that the slope of the Pepperberg plot is determined by arrestin binding. Because the maximum reduction of  $\tau_E$  and  $\tau_R$  by light adaptation could reach eightfold (Figs. 7 and 10), the effect of the turn-off acceleration seems sufficient to account for the maximum 85-fold desensitization observed experimentally.

As already said, the desensitization by steady background observed in frog rods significantly exceeds the desensitization obtained in salamander in a similar sort of experiments. It seems that salamander (and perhaps mouse) rods lack some mechanism(s) that allow frog rods to adapt to a wide range of light intensities. This is in line with findings in the bullfrog where 3,000-fold sensitivity reduction to steady illumination during light adaptation was observed and also partly attributed to the reduced lifetimes of active intermediates (Calvert et al., 2002).

In summary, we show here that light adaptation accelerates both turn-off processes that shape the main phase of the PDE response. This suggests that not only rhodopsin but also transducin quenching is under light adaptation control in frog rods. The acceleration may reach eightfold and is sufficient to account for an  $\approx 80$ -fold sensitivity reduction observed in Pepperberg-type experiments. No regulation of the phototransduction gain (in Lamb and Pugh, 1992 sense) is involved. The process that controls recovery from saturating flashes and sets the so-called dominant time constant is adaptation independent and is not that of either rhodopsin phosphorylation or transducin shut-off that shapes responses to nonsaturating stimuli. It is tentatively identified with arresting binding to rhodopsin partially inactivated by phosphorylation. The biochemical mechanisms that underlie the regulation of the lifetime of active transducin by light adaptation remain to be elucidated.

## APPENDIX

The goal of the Appendix is to derive the equations that describe the time course of flash-induced PDE activity

under the assumption that the cascade shut-off is a three-stage process. The kinetic scheme that we consider here is a truncated version of a more complete scheme by Firsov et al. (2005).

Fully activated rhodopsin generated by a flash ( $R_0^*$ ) is capable of producing an active transducin-GTP-phosphodiesterase complex ( $T \cdot GTP \cdot PDE^*$ ) at the rate of  $\nu_{RE}$ . Simultaneously,  $R^*$  is inactivated by phosphorylation to  $R_P$ , with the time constant of  $\tau_R$ . Phosphorylation reduces its activity toward transducin to  $a \cdot \nu_{RE}$ , where  $a < 1$ .  $R_P$  is completely quenched by arrestin binding that proceeds with the time constant of  $\tau_A$ . Active  $T \cdot GTP \cdot PDE^*$  is quenched by transducin GTP-ase with the time constant of  $\tau_E$ .

Obviously,

$$R^*(t) = R_0^* \cdot \exp(-t/\tau_R). \quad (1a)$$

Concentration of  $R_P$  is given by

$$R_P(t) = R_0^* \frac{\tau_A}{\tau_R - \tau_A} (\exp(-t/\tau_R) - \exp(-t/\tau_A)). \quad (2a)$$

Concentration of active PDE\* originating from  $R^*$  is given by the convolution of Eq. 1a with  $\exp(-t/\tau_E)$ , multiplied by  $\nu_{RE}$ :

$$P_1(t) = R_0^* \cdot \nu_{RE} \frac{\tau_R \cdot \tau_E}{\tau_R - \tau_E} (\exp(-t/\tau_R) - \exp(-t/\tau_E)). \quad (3a)$$

In the special case of  $\tau_R = \tau_E = \tau$ ,

$$P_1(t) = R_0^* \cdot \nu_{RE} \cdot t \cdot \exp(-t/\tau). \quad (4a)$$

Similarly, PDE\* originating from  $R_P$  is the convolution of Eq. 2a with  $\exp(-t/\tau_E)$ , multiplied by  $a \cdot \nu_{RE}$ :

$$P_2(t) = R_0^* \frac{a \cdot \nu_{RE} \tau_A}{\tau_R - \tau_A} \left( \frac{\tau_E \tau_R}{\tau_E - \tau_R} (\exp(-t/\tau_E) - \exp(-t/\tau_R)) - \frac{\tau_A \tau_E}{\tau_A - \tau_E} (\exp(-t/\tau_A) - \exp(-t/\tau_E)) \right). \quad (5a)$$

Total PDE\* coming via the two pathways is

$$PDE^*(t) = P_1(t) + P_2(t). \quad (6a)$$

Assuming that the recovery from saturation occurs when  $PDE^*(t)$  drops to a certain criterion level  $C$ ,  $T_{sat}$  can be found by solving  $PDE^*(t) = C$  with respect to  $t$ . This cannot be done analytically. However, a series of  $R_0^*$  values corresponding to various  $t = T_{sat}$  can be computed, and then x and y axes swapped to obtain  $T_{sat}$  versus  $R_0^*$  plot similar to Fig. 11.

This work is supported by the Russian Foundation for Basic Research grant 05-04-49064 (to M.L. Firsov) and by a grant from the Biological Division of the Russian Academy of Sciences (to V.I. Govardovskii).

Olaf S. Andersen served as editor.

Submitted: 30 April 2008

Accepted: 9 October 2008

## REFERENCES

- Angleon, J.K., and T.G. Wensel. 1993. A GTPase-accelerating factor for transducin, distinct from its effector cGMP phosphodiesterase, in rod outer segment membranes. *Neuron*. 11:939–949.
- Arshavsky, V.Y., and M.D. Bownds. 1992. Regulation of deactivation of photoreceptor G protein by its target enzyme and cGMP. *Nature*. 357:416–417.
- Arshavsky, V.Y., T.D. Lamb, and E.N. Pugh Jr. 2002. G proteins and phototransduction. *Annu. Rev. Physiol.* 64:153–187.
- Balasubramanian, N., K. Levay, T. Keren-Raifman, E. Faurobert, and V.Z. Slepak. 2001. Phosphorylation of the regulator of G protein signaling RGS9-1 by protein kinase A is a potential mechanism of light- and  $Ca^{2+}$ -mediated regulation of G protein function in photoreceptors. *Biochemistry*. 40:12619–12627.
- Baylor, D.A., T.D. Lamb, and K.W. Yau. 1979. Responses of retinal rods to single photons. *J. Physiol.* 288:613–634.
- Bennett, N., and A. Sitaramayya. 1988. Inactivation of photoexcited rhodopsin in retinal rods: the roles of rhodopsin kinase and 48-kDa protein (arrestin). *Biochemistry*. 27:1710–1715.
- Burns, M.E., and V.Y. Arshavsky. 2005. Beyond counting photons: trials and trends in vertebrate visual transduction. *Neuron*. 48:387–401.
- Burns, M.E., and D.A. Baylor. 2001. Activation, deactivation, and adaptation in vertebrate photoreceptor cells. *Annu. Rev. Neurosci.* 24:779–805.
- Burns, M.E., A. Mendez, J. Chen, and D.A. Baylor. 2002. Dynamics of cyclic GMP synthesis in retinal rods. *Neuron*. 36:81–91.
- Bush, R.A., and C.L. Makino. 2007. Recoverin shapes the photoreponse of retinal rods. In *Neuronal Calcium Sensor Proteins*. P.P. Philippov and K.W. Koch, editors. Nova Science Publishers, NY. 153–180.
- Calvert, P.D., T.W. Ho, Y.M. LeFebvre, and V.Y. Arshavsky. 1998. Onset of feedback reactions underlying vertebrate rod photoreceptor light adaptation. *J. Gen. Physiol.* 111:39–51.
- Calvert, P.D., V.I. Govardovskii, V.Y. Arshavsky, and C.L. Makino. 2002. Two temporal phases of light adaptation in retinal rods. *J. Gen. Physiol.* 119:129–145.
- Caruso, G., P. Bisegna, L. Shen, D. Andreucci, H.E. Hamm, and E. DiBenedetto. 2006. Modeling the role of incisures in vertebrate phototransduction. *Biophys. J.* 91:1192–1212.
- Chabre, M., and P. Deterre. 1989. Molecular mechanism of visual transduction. *Eur. J. Biochem.* 179:255–266.
- Chen, C.K. 2005. The vertebrate phototransduction cascade: amplification and termination mechanisms. *Rev. Physiol. Biochem. Pharmacol.* 154:101–121.
- Chen, C.K., M.E. Burns, W. He, T.G. Wensel, D.A. Baylor, and M.I. Simon. 2000. Slowed recovery of rod photoresponse in mice lacking the GTPase accelerating protein RGS9-1. *Nature*. 403:557–560.
- Cobbs, W.H. 1991. Light and dark active phosphodiesterase regulation in salamander rods. *J. Gen. Physiol.* 98:575–614.
- Doan, T., A. Mendez, P.B. Detwiler, J. Chen, and F. Rieke. 2006. Multiple phosphorylation sites confer reproducibility of the rod's single-photon responses. *Science*. 313:530–533.
- Fain, G.L., T.D. Lamb, H.R. Matthews, and R.L.W. Murphy. 1989. Cytoplasmic calcium concentration as the messenger for light adaptation in salamander rods. *J. Physiol.* 416:215–243.
- Fesenko, E.E., S.S. Kolesnikov, and A.L. Lyubarsky. 1985. Induction by cyclic GMP of cationic conductance in plasma membrane of retinal rod outer segment. *Nature*. 313:310–313.



- Field, G.D., and F. Rieke. 2002. Mechanisms regulating variability of the single photon responses of mammalian rod photoreceptors. *Neuron*. 35:733–747.
- Firsov, M.L., A.V. Kolesnikov, E.Y. Golobokova, and V.I. Govardovskii. 2005. Two realms of dark adaptation. *Vision Res.* 45:147–151.
- Gorodovikova, E.N., A.A. Gimelbrant, I.I. Senin, and P.P. Philippov. 1994. Recoverin mediates the calcium effect upon rhodopsin phosphorylation and cGMP hydrolysis in bovine retina rod cells. *FEBS Lett.* 349:187–190.
- Gray-Keller, M.P., and P.B. Detwiler. 1994. The calcium feedback signal in the phototransduction cascade of vertebrate rods. *Neuron*. 13:849–861.
- Gray-Keller, M.P., and P.B. Detwiler. 1996.  $\text{Ca}^{2+}$  dependence of dark- and light-adapted flash responses in rod photoreceptors. *Neuron*. 17:323–331.
- Hamer, R.D. 2000a. Computational analysis of vertebrate phototransduction: combined quantitative and qualitative modeling of dark- and light-adapted responses in amphibian rods. *Vis. Neurosci.* 17:679–699.
- Hamer, R.D. 2000b. Analysis of  $\text{Ca}^{++}$ -dependent gain changes in PDE activation in vertebrate rod phototransduction. *Mol. Vis.* 6:265–286.
- Hamer, R.D., S.C. Nicholas, D. Tranchina, P.A. Liebman, and T.D. Lamb. 2003. Multiple steps of phosphorylation of activated rhodopsin can account for the reproducibility of vertebrate rod single-photon responses. *J. Gen. Physiol.* 122:419–444.
- Hamer, R.D., S.C. Nicholas, D. Tranchina, T.D. Lamb, and J.L. Jarvinen. 2005. Toward a unified model of vertebrate rod phototransduction. *Vis. Neurosci.* 22:417–436.
- Haynes, L.W., A.R. Kay, and K.W. Yau. 1986. Single cyclic GMP-activated channel activity in excised patches of rod outer segment membrane. *Nature*. 321:66–70.
- He, W., C.W. Cowan, and T.G. Wensel. 1998. RGS9, a GTPase accelerator for phototransduction. *Neuron*. 20:95–102.
- Hodgkin, A.L., and B.J. Nunn. 1988. Control of light-sensitive current in salamander rods. *J. Physiol.* 403:439–471.
- Hodgkin, A.L., P.A. McNaughton, and B.J. Nunn. 1985. The ionic selectivity and calcium dependence of the light-sensitive pathway in toad rods. *J. Physiol.* 358:447–468.
- Hu, G., G.F. Jang, C.W. Cowan, T.G. Wensel, and K. Palczewski. 2001. Phosphorylation of RGS9-1 by an endogenous protein kinase in rod outer segments. *J. Biol. Chem.* 276:22287–22295.
- Jindrova, H., and P.B. Detwiler. 2000. Cyclic AMP has no effect on the generation, recovery, or background adaptation of light responses in functionally intact rod outer segments: with implications about the function of phosducin. *Vis. Neurosci.* 17:887–892.
- Kennedy, M.J., M.E. Sowa, T.G. Wensel, and J.B. Hurley. 2003. Acceleration of key reactions as a strategy to elucidate the rate-limiting chemistry underlying phototransduction inactivation. *Invest. Ophthalmol. Vis. Sci.* 44:1016–1022.
- Krispel, C.M., C.K. Chen, M.I. Simon, and M.E. Burns. 2003. Novel form of adaptation in mouse retinal rods speeds recovery of phototransduction. *J. Gen. Physiol.* 122:703–712.
- Krispel, C.M., D. Chen, N. Melling, Y.J. Chen, K.A. Martemyanov, N. Quillinan, V.Y. Arshavsky, T.G. Wensel, C.K. Chen, and M.E. Burns. 2006. RGS expression rate-limits recovery of rod photoreceptors. *Neuron*. 51:409–416.
- Kuzmin, D.G., M.L. Firsov, and V.I. Govardovskii. 2004. Mathematical modeling of phototransduction and light adaptation in frog retinal rods. *Sens. Syst.* 18:305–316.
- Lamb, T.D., and E.N. Pugh Jr. 1992. A quantitative account of the activation steps involved in phototransduction in amphibian photoreceptors. *J. Physiol.* 449:719–758.
- Lyubarsky, A., S. Nikonov, and E.N. Pugh Jr. 1996. The kinetics of inactivation of the rod phototransduction cascade with constant  $\text{Ca}^{2+}$ . *J. Gen. Physiol.* 107:19–34.
- Makino, E.R., J.W. Handy, T. Li, and V.Y. Arshavsky. 1999. The GTPase activating factor for transducin in rod photoreceptors is the complex between RGS9 and type 5 G protein beta subunit. *Proc. Natl. Acad. Sci. USA*. 96:1947–1952.
- Matthews, H.R. 1995. Effect of lowered cytoplasmic calcium concentration and light on the responses of salamander rod photoreceptors. *J. Physiol.* 484:267–286.
- Matthews, H.R. 1996. Static and dynamic actions of cytoplasmic  $\text{Ca}^{2+}$  in the adaptation of responses to saturating flashes in salamander rods. *J. Physiol.* 490:1–15.
- Matthews, H.R. 1997. Actions of  $\text{Ca}^{2+}$  on an early stage in phototransduction revealed by the dynamic fall in  $\text{Ca}^{2+}$  concentration during the bright flash response. *J. Gen. Physiol.* 109:141–146.
- Matthews, H.R., and G.L. Fain. 2001. A light-dependent increase in free  $\text{Ca}^{2+}$  concentration in the salamander rod outer segment. *J. Physiol.* 532:305–321.
- Matthews, H.R., R.L. Murphy, G.L. Fain, and T.D. Lamb. 1988. Photoreceptor light adaptation is mediated by cytoplasmic calcium concentration. *Nature*. 334:67–69.
- Matthews, H.R., R.L. Murphy, G.L. Fain, and T.D. Lamb. 1990. Light adaptation in cone photoreceptors of the salamander: a role for cytoplasmic calcium. *J. Physiol.* 420:447–469.
- Murnick, J.G., and T.D. Lamb. 1996. Kinetics of desensitization induced by saturating flashes in toad and salamander rods. *J. Physiol.* 495:1–13.
- Nakatani, K., and K.W. Yau. 1988. Calcium and light adaptation in retinal rods and cones. *Nature*. 334:69–71.
- Nekrasova, E.R., D.M. Berman, R.R. Rustandi, H.E. Hamm, A.G. Gilman, and V.Y. Arshavsky. 1997. Activation of transducin guanosine triphosphatase by two proteins of the RGS family. *Biochemistry*. 36:7638–7643.
- Nikonov, S., N. Engheta, and E.N. Pugh Jr. 1998. Kinetics of recovery of the dark-adapted salamander rod photoresponse. *J. Gen. Physiol.* 111:7–37.
- Nikonov, S., T.D. Lamb, and E.N. Pugh Jr. 2000. The role of steady phosphodiesterase activity in the kinetics and sensitivity of the light-adapted salamander rod photoresponse. *J. Gen. Physiol.* 116:795–824.
- Nikonov, S., T.D. Lamb, and E.N. Pugh Jr. 2001. Photoreceptor sensitivity and kinetics in light adaptation. *J. Gen. Physiol.* 117:365–366.
- Palczewski, K., G. Rispoli, and P.B. Detwiler. 1992. The influence of arrestin (48K protein) and rhodopsin kinase on visual transduction. *Neuron*. 8:117–126.
- Pepperberg, D.R. 2001. Transduction gain in light adaptation of rod photoreceptors. *J. Gen. Physiol.* 117:361–366.
- Pepperberg, D.R., M.C. Cornwall, M. Kahlert, K.P. Hofmann, J. Jin, G.J. Jones, and H. Ripps. 1992. Light-dependent delay in the falling phase of the retinal rod photoresponse. *Vis. Neurosci.* 8:9–18.
- Pepperberg, D.R., J. Jin, and G.J. Jones. 1994. Modulation of transduction gain in light adaptation of retinal rods. *Vis. Neurosci.* 11:53–62.
- Pugh, E.N. Jr., and T.D. Lamb. 2000. Phototransduction in vertebrate rods and cones: molecular mechanisms of amplification, recovery and light adaptation. In *Handbook of Biological Physics*. D.G. Stavenga, J.E.N. Pugh, and W.J. de Grip, editors. Elsevier Science B.V., Amsterdam. 183–255.
- Rieke, F., and D.A. Baylor. 1998. Origin of reproducibility in the responses of retinal rods to single photons. *Biophys. J.* 75:1836–1857.
- Sagoo, M.S., and L. Lagnado. 1997. G-protein deactivation is rate-limiting for shut-off of the phototransduction cascade. *Nature*. 389:392–395.

- Smith, N.P., and T.D. Lamb. 1997. The  $\alpha$ -wave of the human electroretinogram recorded with a minimally invasive technique. *Vision Res.* 37:2943–2952.
- Sokal, I., G. Hu, Y. Liang, M. Mao, T.G. Wensel, and K. Palczewski. 2003. Identification of protein kinase C isozymes responsible for the phosphorylation of photoreceptor-specific RGS9-1 at Ser475. *J. Biol. Chem.* 278:8316–8325.
- Vishnivetskiy, S.A., D. Raman, J. Wei, M.J. Kennedy, J.B. Hurley, and V.V. Gurevich. 2007. Regulation of arrestin binding by rhodopsin phosphorylation level. *J. Biol. Chem.* 44: 32075–32083.
- Wensel, T.G. 2002. RGS9-1 phosphorylation and  $\text{Ca}^{2+}$ . *Adv. Exp. Med. Biol.* 514:125–129.
- Whitlock, G.G., and T.D. Lamb. 1999. Variability in the time course of single photon responses from toad rods: termination of rhodopsin's activity. *Neuron.* 23:337–351.
- Wilden, U., S.W. Hall, and H. Kuhn. 1986. Phosphodiesterase activation by photoexcited rhodopsin is quenched when rhodopsin is phosphorylated and binds the intrinsic 48-kDa protein of rod outer segments. *Proc. Natl. Acad. Sci. USA.* 83:1174–1178.
- Woodruff, M.L., K.M. Janisch, I.V. Peshenko, A.M. Dizhoor, S.H. Tsang, and G.L. Fain. 2008. Modulation of phosphodiesterase6 turnoff during background illumination in mouse rod photoreceptors. *J. Neurosci.* 28:2064–2074.
- Xu, J., R.L. Dodd, C.L. Makino, M.I. Simon, D.A. Baylor, and J. Chen. 1997. Prolonged photoresponses in transgenic mouse rods lacking arrestin. *Nature.* 389:505–509.
- Younger, J.P., S.T. McCarthy, and W.G. Owen. 1996. Light-dependent control of calcium in intact rods of the bullfrog *Rana catesbeiana*. *J. Neurophysiol.* 75:354–366.
- Zimmerman, A.L., and D.A. Baylor. 1986. Cyclic GMP-sensitive conductance of retinal rods consists of aqueous pores. *Nature.* 321:70–72.